AD-A081 421 LITTON SYSTEMS INC WOODLAND HILLS CA GUIDANCE AND CO--ETC F/G 17/7
MULTIOSCILLATOR LASER GYRO STUDY.(U)
JAN 80 V E SANDERS F33615-78-C-1524

UNCLASSIFIED AFAL-TR-79-1214 NL

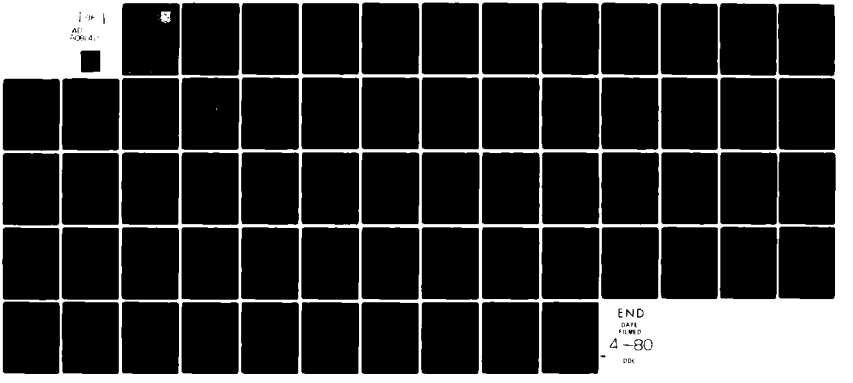

END
DATE FILMED
4-80
DDC

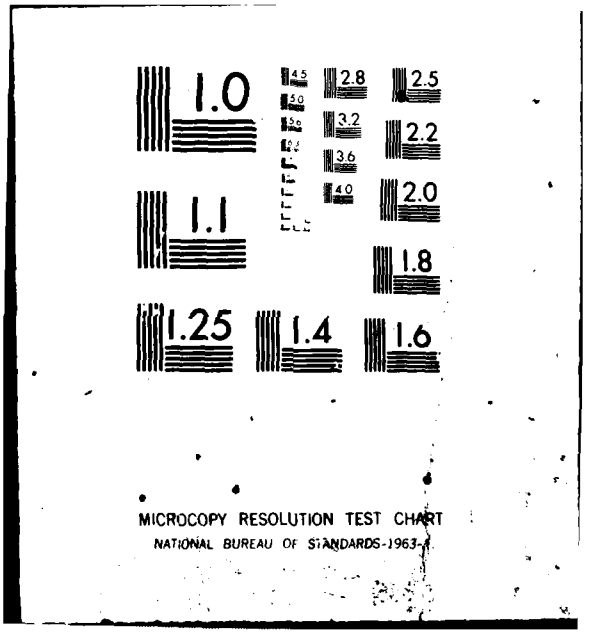
1.0
1.1
1.25
1.4
1.6
1.8
2.0
2.2
2.5
2.8
3.2
3.6
4.0
4.5
5.0
MICROCOPY RESOLUTION TEST CHART
NATIONAL BUREAU OF STANDARDS-1963-A

AFAL-TR-79-1214

LEVEL

AD A081421

MULTIMODELLA FOR LASER GYRO STUDY

Litton, Guidance & Control Systems
5500 Canoga Avenue
Woodland Hills, California 91365

January 1980

TECHNICAL REPORT AFAL-TR-79-1214
Final Report for Period Sept 1978 - Sept 1979

Approved for public release; distribution unlimited

DTIC
SELECTED
S D
A

FILE COPY

NOTICE

When Government drawings, specifications, or other data are used for any purpose other than in connection with a definitely related Government procurement operation, the United States Government thereby incurs no responsibility nor any obligation whatsoever; and the fact that the government may have formulated, furnished, or in any way supplied the said drawings, specifications, or other data, is not to be regarded by implication or otherwise as in any manner licensing the holder or any other person or corporation, or conveying any rights or permission to manufacture, use, or sell any patented invention that may in any way be related thereto.

This report has been reviewed by the Information Office (OI) and is releasable to the National Technical Information Service (NTIS). At NTIS, it will be available to the general public, including foreign nations.

This technical report has been reviewed and is approved for publication.

David W. Pleva

DAVID W. PLEVA
Project Engineer

Robert E. Witters

ROBERT E. WITTERS,
Technical Manager

FOR THE COMMANDER

Ronald L. Ringo

RONALD L. RINGO
Branch Chief

"If your address has changed, if you wish to be removed from our mailing list, or if the addressee is no longer employed by your organization please notify AFWAL/MLBA, W-PAFB, OH 45433 to help us maintain a current mailing list".

Copies of this report should not be returned unless return is required by security considerations, contractual obligations, or notice on a specific document.

AIR FORCE/56780/7 Nov 86—300

SECURITY CLASSIFICATION OF THIS PAGE *(When Data Entered)*

REPORT DOCUMENTATION PAGE

READ INSTRUCTIONS BEFORE COMPLETING FORM

1. REPORT NUMBER: AFAL-TR-79-1214	2. GOVT ACCESSION NO.
3. RECIPIENT'S CATALOG NUMBER	
4. TITLE *(and Subtitle)*: MULTIOSCILLATOR LASER GYRO STUDY.	5. TYPE OF REPORT & PERIOD COVERED: Final rept. Sep 78 - Sep 79
6. PERFORMING ORG. REPORT NUMBER	
7. AUTHOR(s): V. E. Sanders	8. CONTRACT OR GRANT NUMBER(s): F33615-78-C-1524
9. PERFORMING ORGANIZATION NAME AND ADDRESS: Litton, Guidance & Control Systems, 5500 Canoga Ave, Woodland Hills, California 91365	10. PROGRAM ELEMENT, PROJECT, TASK AREA & WORK UNIT NUMBERS: 2305 R3 03
11. CONTROLLING OFFICE NAME AND ADDRESS: United States Air Force, AFAL (RWA), Wright Patterson AFB, Ohio 45433	12. REPORT DATE: Jan 1980
	13. NUMBER OF PAGES: 62
14. MONITORING AGENCY NAME & ADDRESS *(if different from Controlling Office)*: (Same)	15. SECURITY CLASS. *(of this report)*: UNCLASSIFIED
	15a. DECLASSIFICATION DOWNGRADING SCHEDULE

16. DISTRIBUTION STATEMENT *(of this Report)*

Approved for public release, distribution unlimited

17. DISTRIBUTION STATEMENT *(of the abstract entered in Block 20, if different from Report)*

(Same)

18. SUPPLEMENTARY NOTES

19. KEY WORDS *(Continue on reverse side if necessary and identify by block number)*

Laser Gyros
Multioscillator Gyros
Gyroscopes
Guidance
Navigation

20. ABSTRACT *(Continue on reverse side if necessary and identify by block number)*

Parameter variation experiments were conducted and results are reported on the Litton IR&D developed LG2432 multioscillator laser gyro. The purpose in this collection of data is in its intended use as an aid in the advancement of a developing multioscillator theoretical model. The model predicts both the

DD FORM 1 JAN 73 1473 EDITION OF 1 NOV 65 IS OBSOLETE

SECURITY CLASSIFICATION OF THIS PAGE *(When Data Entered)*

401044

Output intensities and oscillation frequencies of the various ring laser modes in this device. Therefore, the parameter variation experiments are concerned with the intensities and frequencies of the laser modes as a function of several laser gyro environmental parameters. Results from the refined theory and the correlation with the experimental data are discussed.

TABLE OF CONTENTS

LIST OF ILLUSTRATIONS

LIST OF ILLUSTRATIONS (cont)

SECTION I
STUDY, PURPOSE AND OBJECTIVE

The object of this multioscillator ring laser gyro study was to obtain a comprehensive collection of data from a carefully conducted set of parameter variation experiments. The purpose of this collection of data is its intended use as an aid in the advancement of a developing theoretical model. This information may be used to establish the range and magnitudes of various theoretical parameter variables through comparison of model predictions and experimental data.

To accomplish this task and to guide and direct the nature of these experiments, there was a continuous cooperative effort and exchange of data with the corresponding developing theory effort at the University of Arizona, Tucson, through Professor Marlan O. Scully. Correlation discussions where held monthly to review data and to determine the status of the theory. The result from each of these meetings was the formulation of experiments which would yield data needed to support the developing model.

SECTION II
INTRODUCTION AND BACKGROUND

The multioscillator laser gyro concept involves simultaneous laser oscillation of four running-waves in a ring laser. The concept is characterized by its optical biasing scheme allowing angular rotation rate information to be obtained from a difference-frequency beat-note associated with all four oscillating laser modes. Early work by deLang[1] indicate the conceptual scheme. Later workers[2] attained the four simultaneous running-waves in a ring cavity and demonstrated the concept.

The theory referred to herein is that of a Zeeman four-mode ring-laser gyro.[3] This theory is being generated by extending the 1964 Lamb[4] semi-classical scalar theory of a two-mirror standing-wave electric field laser. The developing model considers simultaneous oscillation of four running-wave electric field eigenstates of a single longitudinal and transverse ring-cavity resonant mode, magnetic sublevels of a multi-isotope active gain medium in an arbitrary oriented magnetic field, and an optically anisotropic and nonreciprocal cavity with sources causing loss and scattering of light within the cavity. The most general case in this four-mode problem involves the simultaneous solution of eight coupled differential equations. Two equations describe the dynamics of each vector field: one for the frequency and one for the amplitude.

The biasing of a four-mode gyro differs from that of a two-mode gyro in that it may be static and passive. The biasing is static in that in the absence of rotation the induced frequency splittings between the four oscillating modes are constant. The bias is passive in that the frequency splittings are accomplished with nonmoving elements which are not power consuming

(true strapdown). The biasing involves two types of polarization anisotropic biasing elements in the laser cavity, one reciprocal and one nonreciprocal. Crystal quartz may be used as one of the biasing elements (reciprocal). This element is constructed and oriented in the laser cavity such that the laser beam may propagate along the optic axis of the crystal. The other (nonreciprocal) type of biasing involves the magnetic field Faraday type of optical phenomena. The magnetic field may, for example, be placed on the crystal, or on the active gain media.

Figure 1 illustrates the laser oscillation spectrum of the multioscillator laser gyro used in this study. f_i is the optical frequency of the i'th polarization-propagation direction eigenstate. L and R represent left and right circular polarization and C and A represent the clockwise and anticlockwise directions of propagation. The relative arrangement of the frequencies is a function of the two biasing elements used in these experiments, namely: quartz crystal and magnetic field on the gas plasma. The frequency splitting from the crystal is considerably greater than from the Faraday bias.

The frequency splittings of the four modes is such that effectively two two-mode static biased laser gyros are established in the single ring laser cavity:

Gyro 1:

$$\Delta f \text{ (beat-note)} = f_2 - f_1 \simeq -K\Omega + \text{FARADAY BIAS} \qquad (1)$$

Gyro 2:

$$\Delta f \text{ (beat-note)} = f_4 - f_3 \simeq K\Omega + \text{FARADAY BIAS} \qquad (2)$$

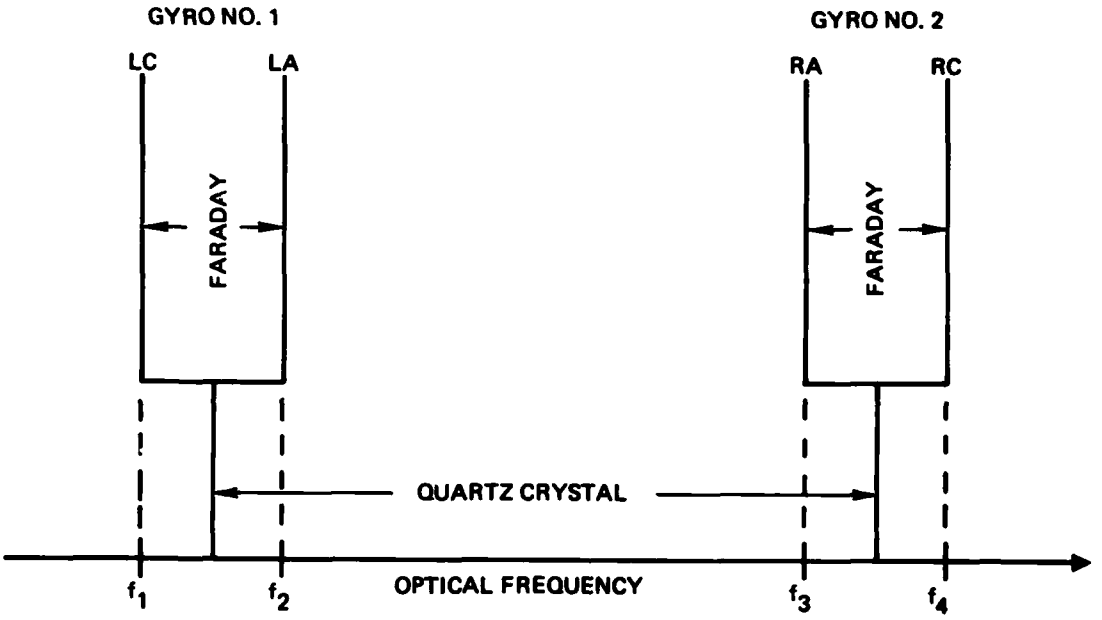

Figure 1. Multioscillator Frequency Spectrum

K is a constant scale factor and Ω is angular velocity of the laser cavity. The scale factor, K, is the familiar two-mode laser gyro scale factor. The difference between these two two-mode beat-notes is the multioscillator beat-note, $\dot{\psi}$, where (see Figure 2):

$$\dot{\psi} \equiv f_4 - f_3 - f_2 + f_1 \simeq 2K\Omega \qquad (3)$$

Note that this beat note has twice the sensitivity to rotation of a two mode laser gyro and the sensitivity to the bias cancels.

Like other laser gyro concepts, the individual oscillating frequency of each mode is not only affected by the biasing and rotation but also by various active coupling phenomena to each of the other modes and by self interaction with the active gain media. The effects of these various phenomena lead to errors in the gyro output. The complexity of the four-mode theory and the functional relations between the various parameters are significantly increased when the magnetic field is applied to the active gain media as compared to the field being applied to the crystal. Nevertheless, application of the magnetic field to the gain media significantly simplifies the mechanical construction complexity of the device. Thus, there is a motivation for considering a multioscillator with field on the active gain media and for extending the present state of four-mode laser gyro theory. For this case, the fully developed complex vector theory is necessary as a design tool in the development of this instrument.

As mentioned earlier, the theory predicts both intensities and frequencies of the various modes. The intensities may be measured directly. However, the frequencies may not be measured

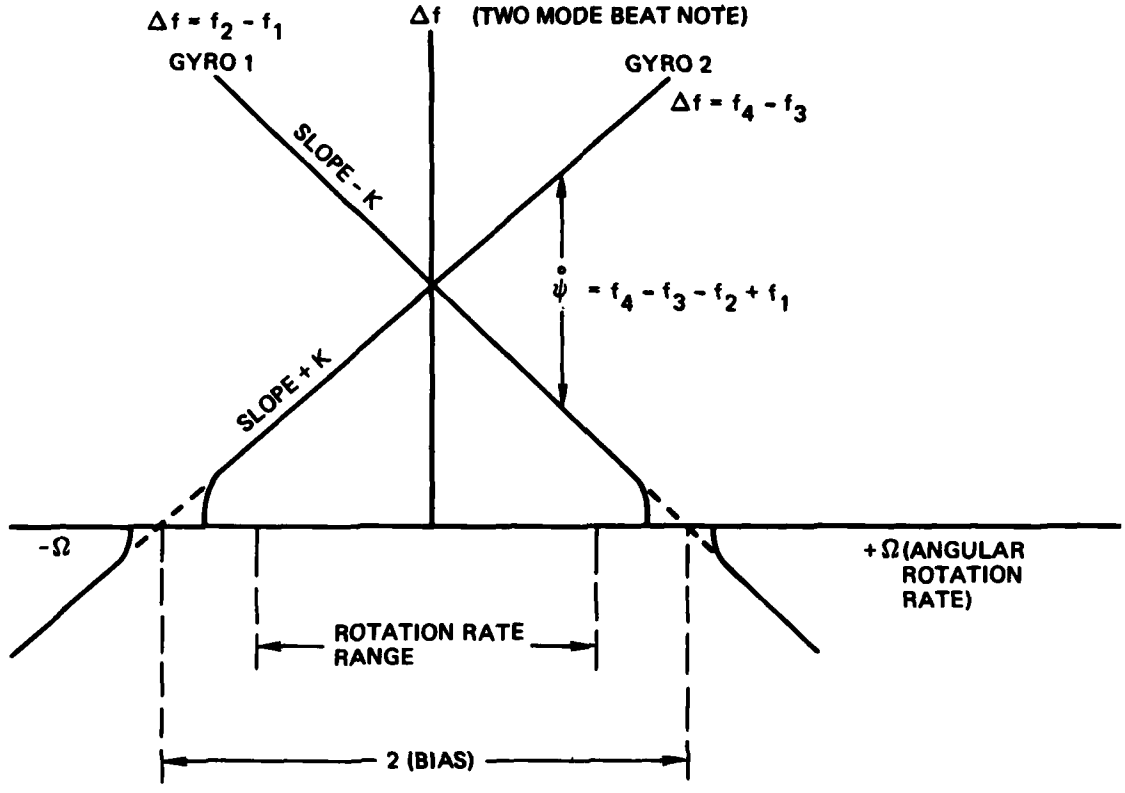

Figure 2. Multioscillator Response to Rotation in Inertial Space

directly with enough accuracy for a useful correlation with the theory. Therefore, difference-frequency beat-notes are most useful in this application. The $\dot{\psi}$ beat-note as defined above is a particularly good choice for a parameter evaluation of a multioscillator gyro and as a means for data correlation with the frequency predictions of the four-mode vector theory.

In addition to the field amplitude and frequency data-theory correlation, a separate study was conducted concerning the electric field polarization characteristics of a multioscillator. This study was reported in Optics Communications, 29, 227 (May 1979). A reprint of this article entitled "Polarization Characteristics of an Anisotropic Ring Laser" is found in Appendix A.

SECTION III
EXPERIMENTAL APPARATUS

The He-Ne ring laser (λ6328Å) apparatus used in this study was the Litton IR&D developed, LG-2432 multioscillator. This instrument was designed to perform a variety of four-mode laser gyro parameter variation experiments. The body of the device was constructed from a solid block of CerVit. Machined into the block are clearance holes, gain bores, and an aperture to accommodate both the optical and electrical discharge paths. Both mirrors and electrodes are affixed to polished surfaces on the blocks. (Figure 3 is intended as an aid in the description of this apparatus.) The block has two separate, equal gain-bore regions with a magnetic coil around each. The electrodes (one cathode and two anodes) are positioned such that the magnetic coil covers all and only that portion of the optical cavity with the gas gain plasma. In addition, the block has a port access to the laser beam optical path where a quartz crystal biasing element may be positioned. The closed optical path of this ring laser is approximately 32 centimeters long, and encloses approximately 43 square centimeters. (K, the two-mode laser gyro scale factor, mentioned earlier in equations 1, 2 and 3, is approximatelу equal to 8×10^4 for this instrument.)

A particularly accommodating feature of this LG-2432 instrument, with respect to performing short term parameter variation experiments, is a valved tip-off connection. The ring laser is easily attached to and removed from a vacuum fill station. Therefore, the gas fill parameters are quickly changeable at will.

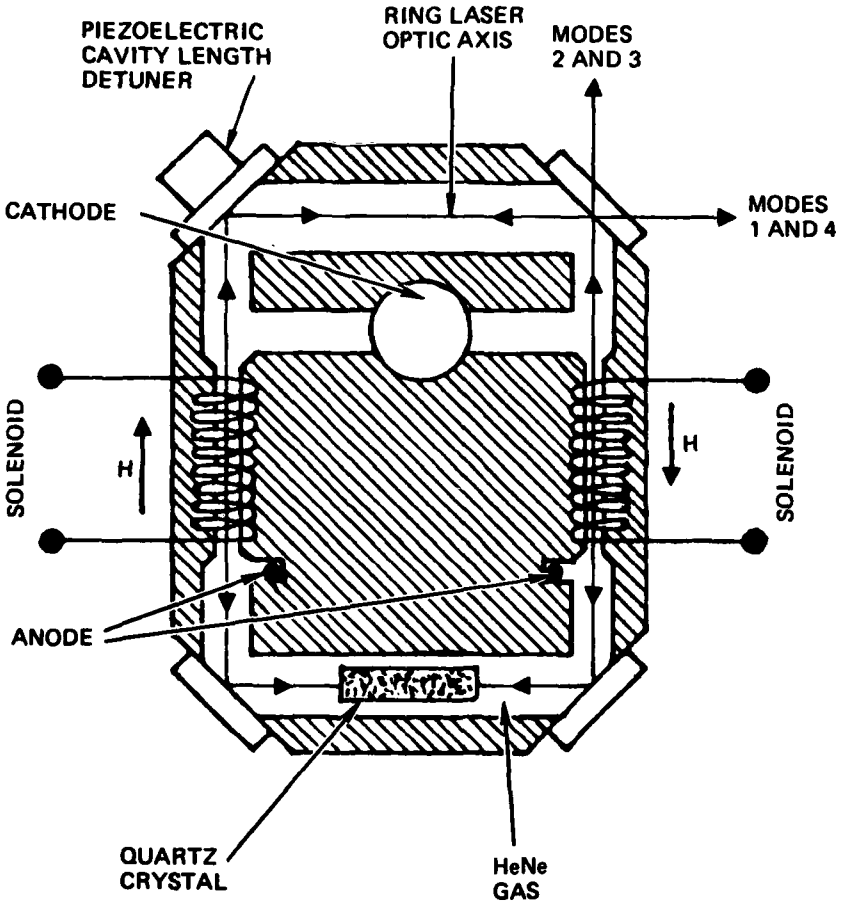

Figure 3. Zeeman Multioscillator Laser Gyro

Alignments of both mirrors and crystal were done with the instrument lasing while attached to a vacuum fill station. The seals on both the mirrors and crystal assembly were wax. When heated, the wax is soft and allows movement of the mirrors or crystal. The mirrors were positioned for maximum intensity output. The crystal orientation was adjusted for maximum circularity of polarization of the output modes. This insures a minimum contribution of birefringence to the total ring cavity from the crystal element. The life time expectancy of a wax-sealed instrument is only a few days. However, this was ample time to do each of the parameter variation experiments.

The original test plan suggested a series of experiments associated with four different crystal element thicknesses. These elements provided the reciprocal type of anisotropic biasing for the frequency splitting between the left and right circularly polarized modes. The four elements provided frequency splittings of: 30, 63, 166, and 440 MHz. These crystals have polished faces nominally perpendicular to the polarization rotary axis with anti-reflection coatings. Each of the crystal elements was constructed from "right handed" quartz; i.e., the optical index of the material is less for right circular polarized light than the index for left circular polarized light. The same is true for propagation in either direction along the rotary axis making the element reciprocal.

In addition to the instrument features mentioned above, one of the cavity mirrors had an attached piezoelectric ceramic device used to control the cavity length. In summation, the ring laser instrument used in this study was capable of variations in the following parameters: magnetic field on the active HeNe plasma (Zeeman effect and Faraday effect) 0-200 gauss, four distinct

polarization rotation elements, cavity length detuning, cavity gain and loss, dual isotope ratio (Ne^{20}/Ne^{22}), He/Ne ratio, gas pressure, linear phase birefringence, and rotation of the cavity in inertial space.

The basic measurement apparatus consists of an optical spectrum analyzer, a photodiode, and a dual-beam oscilloscope in conjunction with various monitoring devices for the above mentioned variable parameters. The functions of these various devices will be discussed in the following descriptions of the various experiments and results.

SECTION IV
EXPERIMENTAL RESULTS

1. Faraday Beat-Note

Figure 4 indicates the magnitude of the frequency splitting from the magnetic field on the gas plasma. The measured beat-note represents the difference frequency between LC and LA or between RC and RA (modes of like polarization) as a function of magnetic field strength.

There are 8 centimeters of the active gas plasma with axial magnetic field. Using this data we calculate a pseudo-Verdet constant of approximately 300 Hz/cm gauss for the gas plasma. The absolute magnitude of the beat-note, magnetic field relation was the same for both the left and right circularly polarized pairs of modes. However, the slopes of the curves were opposite in sign. This accounts for the response of each pair of modes to rotation of the cavity in inertial space as indicated in Figure 2 and the - and + K in equations 1 and 2 respectively.

The significant, measured, laser gyro parameters associated with the data in figure 4 are: One, the polarization ellipticity of all four modes was 1.00 $\pm$0.02 where 1.00 represents circular polarization. This measurement was determined by a ratio of intensity measurements of the major and minor axis of the polarization ellipse. Two, the gain/loss ratio was varied from 1.3 to 1.7. This was varied via the HeNe plasma current. Three, the Ne^{20}/Ne^{22} ratio was approximately 50/50. Four, the He/Ne ratio was approximately 12/1. Five, the total gas pressure is indicated on each of the three curves (2.5, 3.0, 3.7 Torr). Six, the frequency splitting by the crystal was 166 MHz. However, the data was virtually the same for all four crystals. Seven, the cavity length could be varied such that the mean

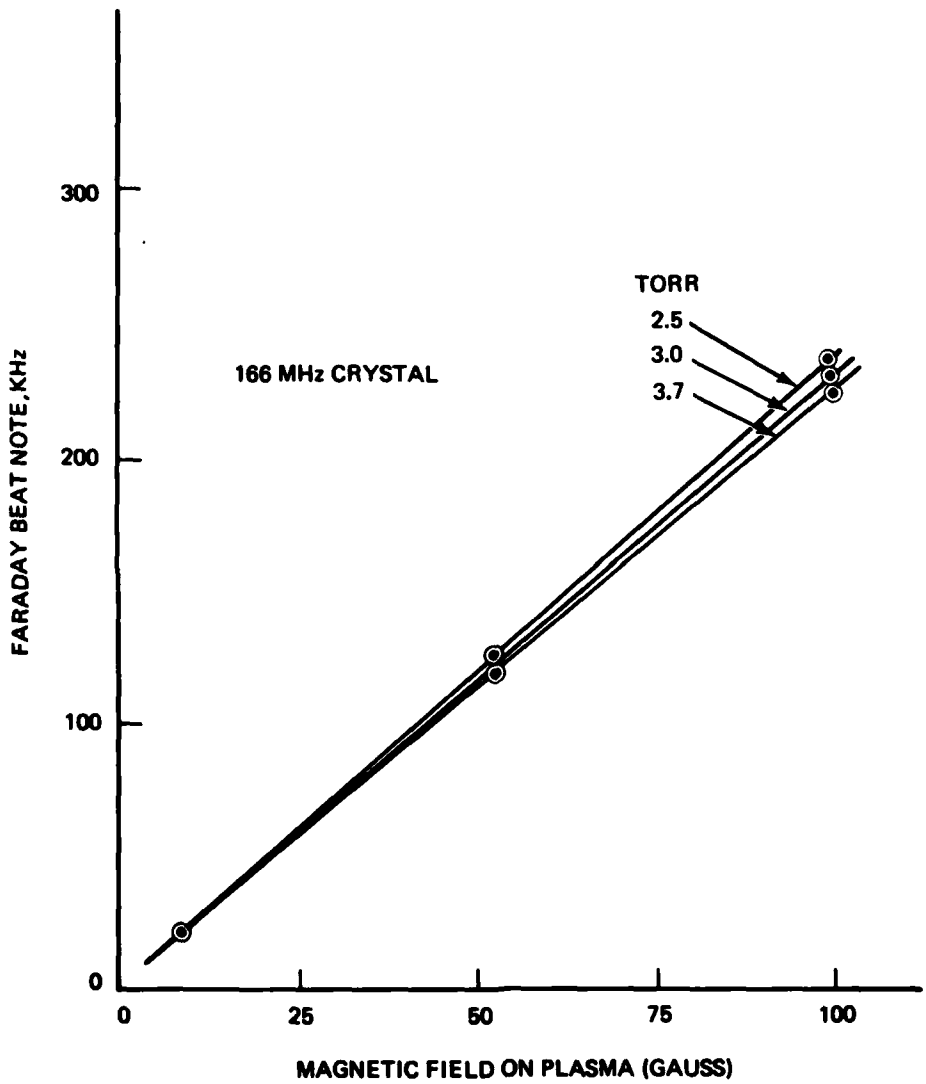

Figure 4. Faraday Beat Note versus Magnetic Field on Gas Plasma

frequency of the two modes could change by ±200 MHz about the center of the gain curve for that pair of modes without affecting the data significantly. Eight, these measurements were made with the instrument attached to the gas fill station; therefore, the rotation in inertial space contribution to this beat-note is insignificant.

The total gas pressure was the only gas-fill parameter that had any significant effect on this beat-note. Variation in the polarization ellipticity of the modes had a significant effect. However, the theoretical model considers only circular polarization. Therefore, this parameter was not varied in any of the experiments. The mirrors and crystals were adjusted in each case for maximum circular polarization.

A. INTENSITY

The following series of figures shows the output intensity of each of the four osillating modes as a function of cavity length tuning and magnetic field on the plasma. The magnitude and direction of the magnetic field is indicated on each graph. The directions of the two fields (one on each plasma gain region) are parallel in that they point in the same direction around the ring cavity as indicated in figure 3. The indicated magnitude of the magnetic field is calculated from the measured current in the coils and is estimated to be accurate to within ±5 percent. The intensity measurements were made with a Spectra-Physics Model 420 Optical Spectrum analyzer. The intensity scale on each graph is unitless and thus is only an indication of the relative intensity, one mode to another, as measured by the optical spectrum analyzer. The output from this same spectrum analyzer also indicates the optical frequency of each mode (accurate to ±10 MHz). The optical frequency tuning was accomplished via the piezo cavity length control device.

In each case zero detuning is the mean optical frequency of all four modes when all four modes are oscillating with equal intensity with zero magnetic field on the plasma. That optical frequency should be near the midpoint of the 6328Å natural transition frequency associated with the two isotopes, Ne^{20} and Ne^{22}. The measured intensity points on each of the graphs for each mode with respect to detuning are: the maximum intensity, the intensity at zero detuning relative to the maximum, and that point on the detuning scale at which lasing oscillation ceases. The shapes of the curves through these points are sketched. The relative intensities as indicated on the graphs should be accurate to within ±5 percent of that indicated by the optical spectrum analyzer output. As before, L and R represent left and right circular polarization and C and A represent clockwise and anticlockwise. The labeling "left and right circular handedness" of the modes is as the modes are in the plasma gain sections of the ring cavity. The crystal being used is also indicated on each graph.

Again, the laser parameters of significance were: One, the polarization ellipticity of each mode was near circular (1.00 ±0.02). Two, the gain/loss ratio was approximately 1.5 at gain maximum for each mode. Three, the Ne^{20}/Ne^{22} isotope ratio was 50/50. Four, the He/Ne ratio was approximately 12/1. Five, the total gas pressure was approximately 3.0 Torr. Six, these measurements were also made with the instrument attached to the fill station.

Intensity measurements associated with the 63 MHz crystal are not indicated due to the fact that they were not significantly different from the ones associated with the 30 MHz crystal.

1. Intensity Figures

All of the curves in figures 5a-i are associated with the 166 MHz crystal:

a. Figure 5a indicates the intensity profile of all four modes without the Zeeman splitting of the gain atoms. Note the curves are reasonably Gaussian with the same curve for LC and LA but different from RC and RA which have the same curve.

b. Figure 5b is associated with 30 gauss in the C direction on the gas plasma gain media. Note the order of the various peak intensities and that the curves are no longer symmetric Gaussian.

c. Figure 5c is associated with 50 gauss in the C direction on the gas plasma gain media. Again note the order of the peaks which is different from the previous figure 4-2b.

d. Figures 5d and e are associated with 70 and 100 gauss respectively. Note the same order of the peaks as the 50 gauss curves and that the deviation from a smooth Gaussian curve becomes more severe as the field magnitude increases.

e. Figures 5h-i are similar to those above except the magnetic field is reversed and points in the A direction around the ring. Note the order of the peaks are different from the corresponding figure with the field in the opposite direction.

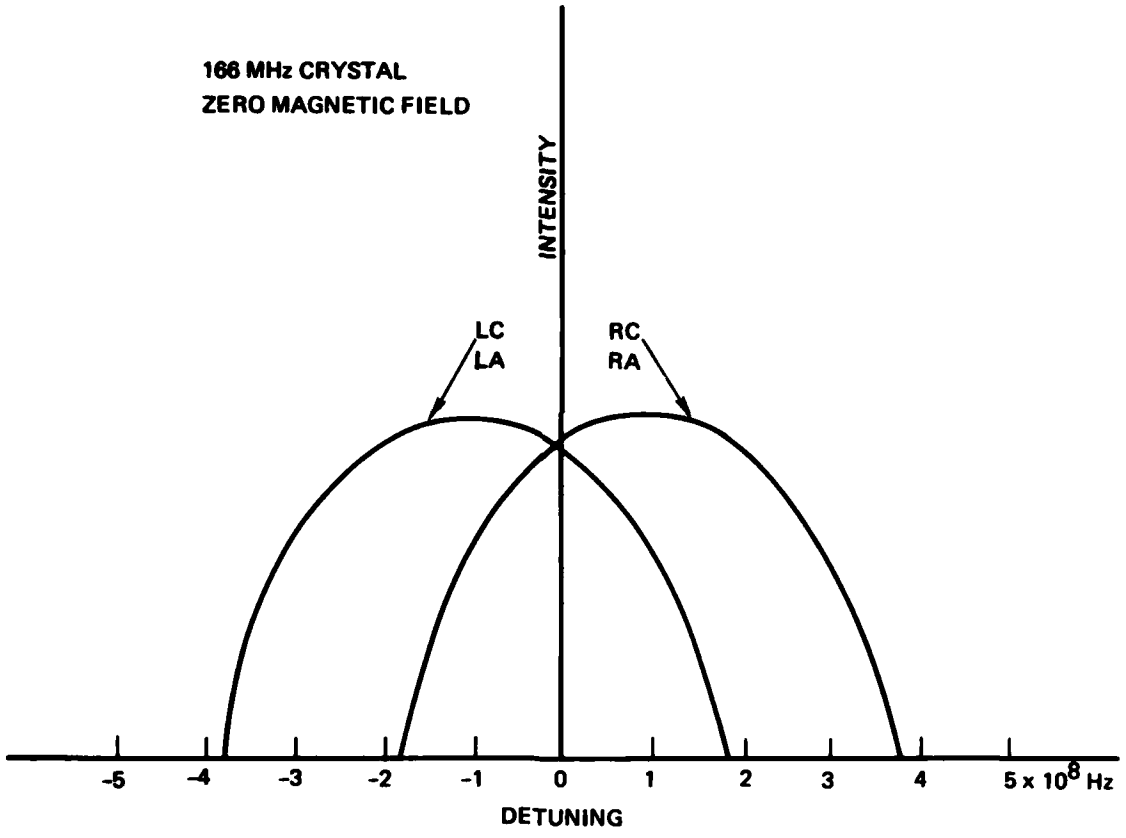

Figure 5a. Intensity versus Cavity Length Tuning

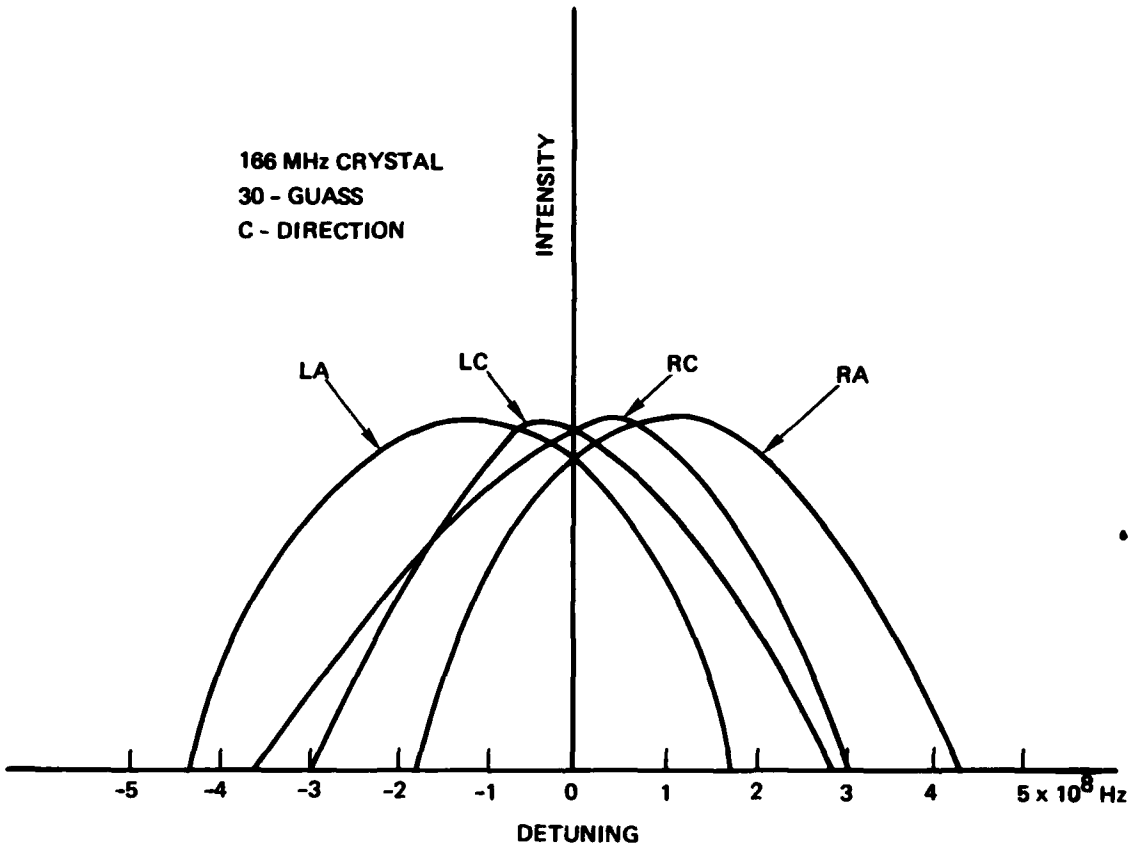

Figure 5b. Intensity versus Cavity Length Tuning

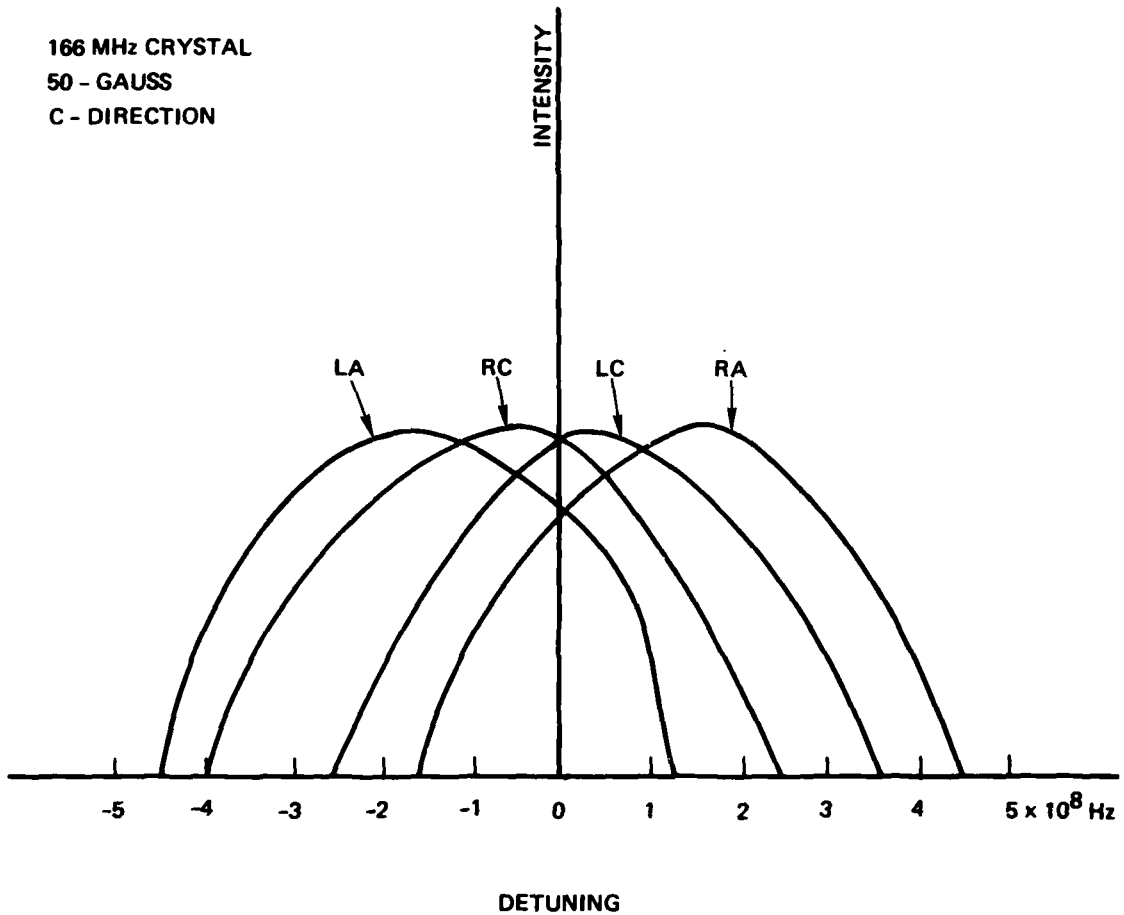

Figure 5c. Intensity versus Cavity Length Tuning

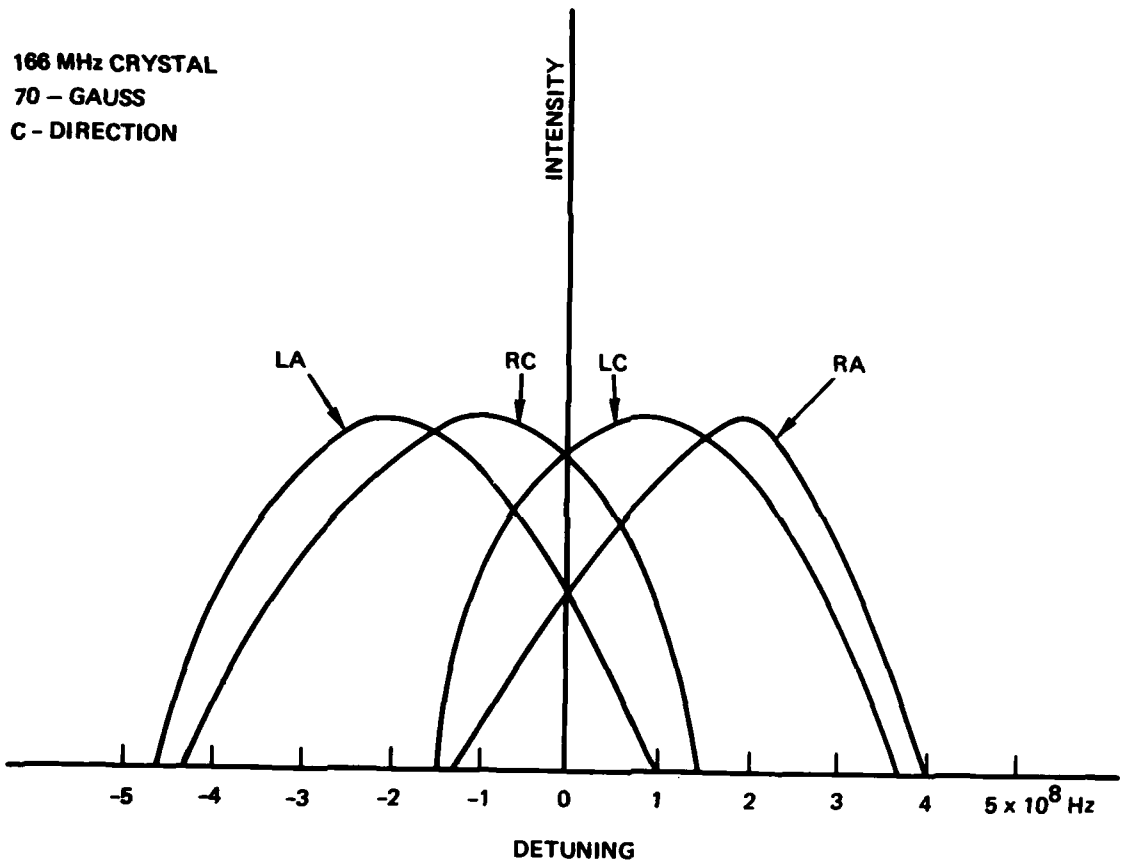

Figure 5d. Intensity versus Cavity Length Tuning

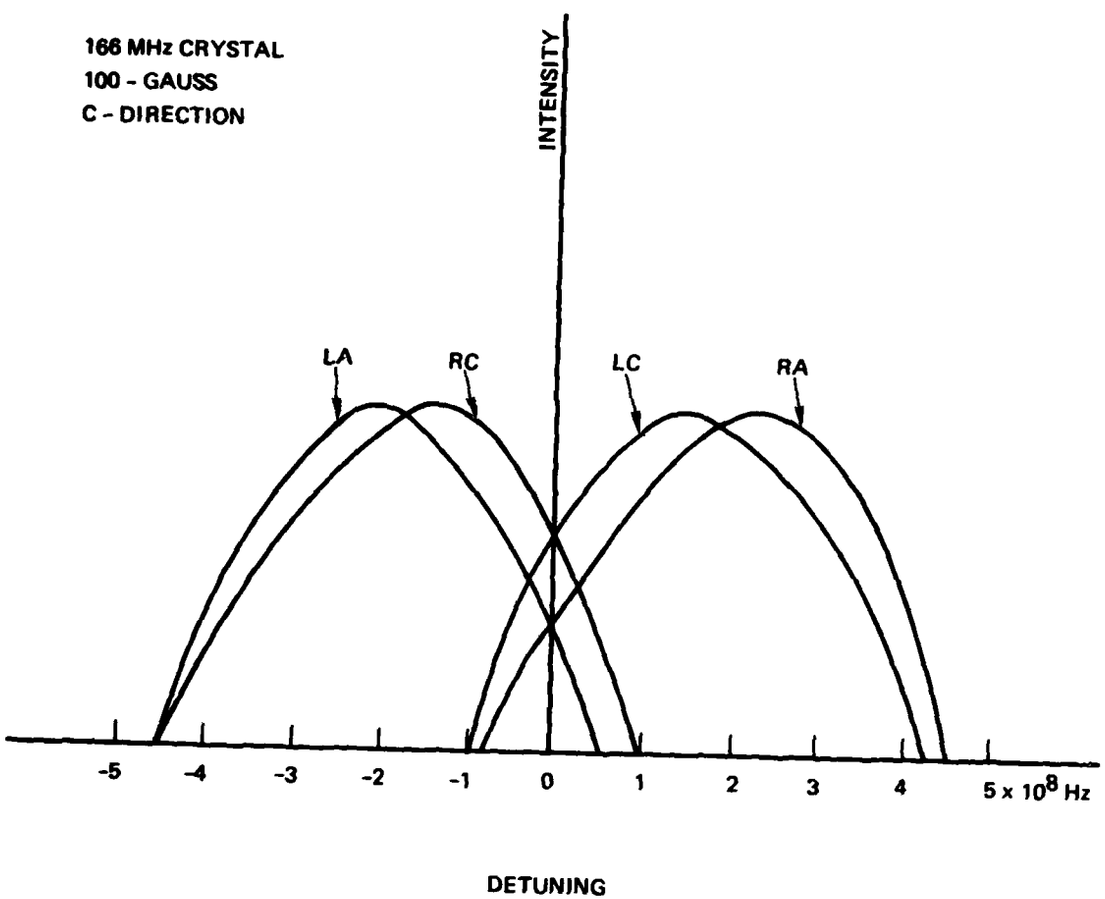

Figure 5e. Intensity versus Cavity Length Tuning

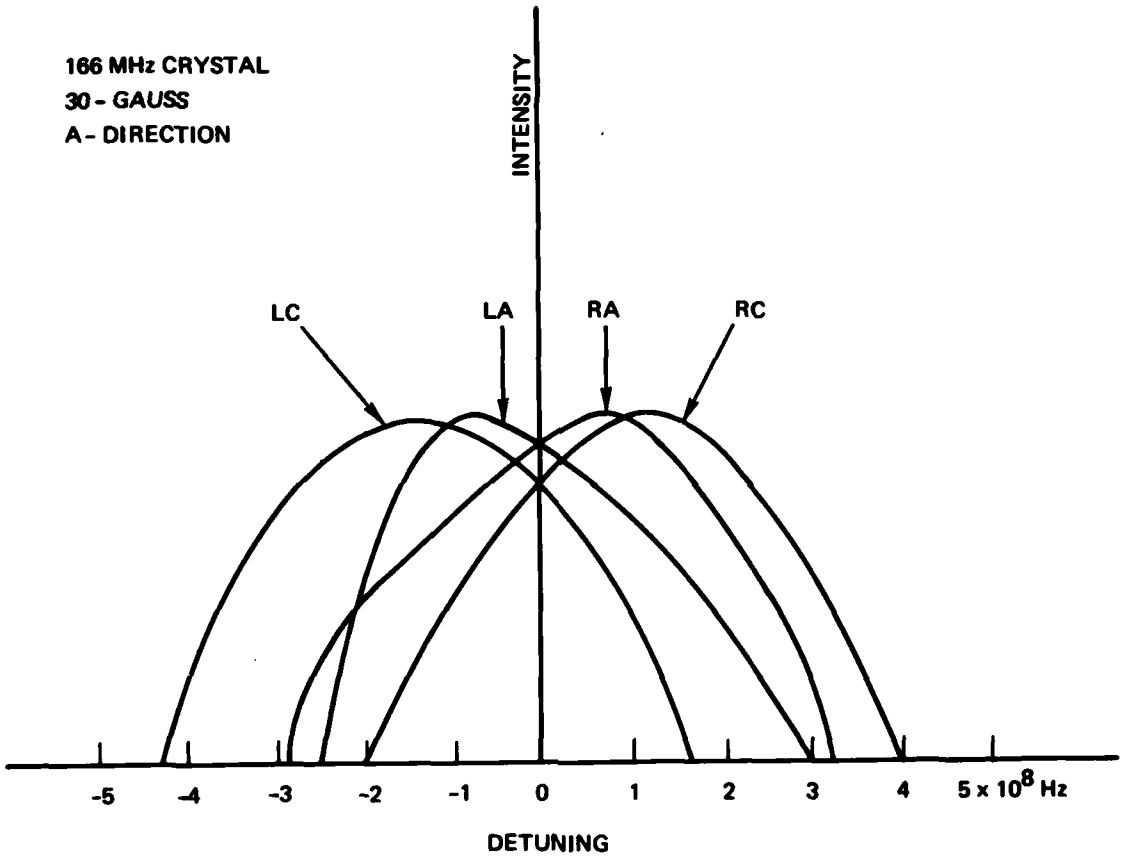

Figure 5f. Intensity versus Cavity Length Tuning

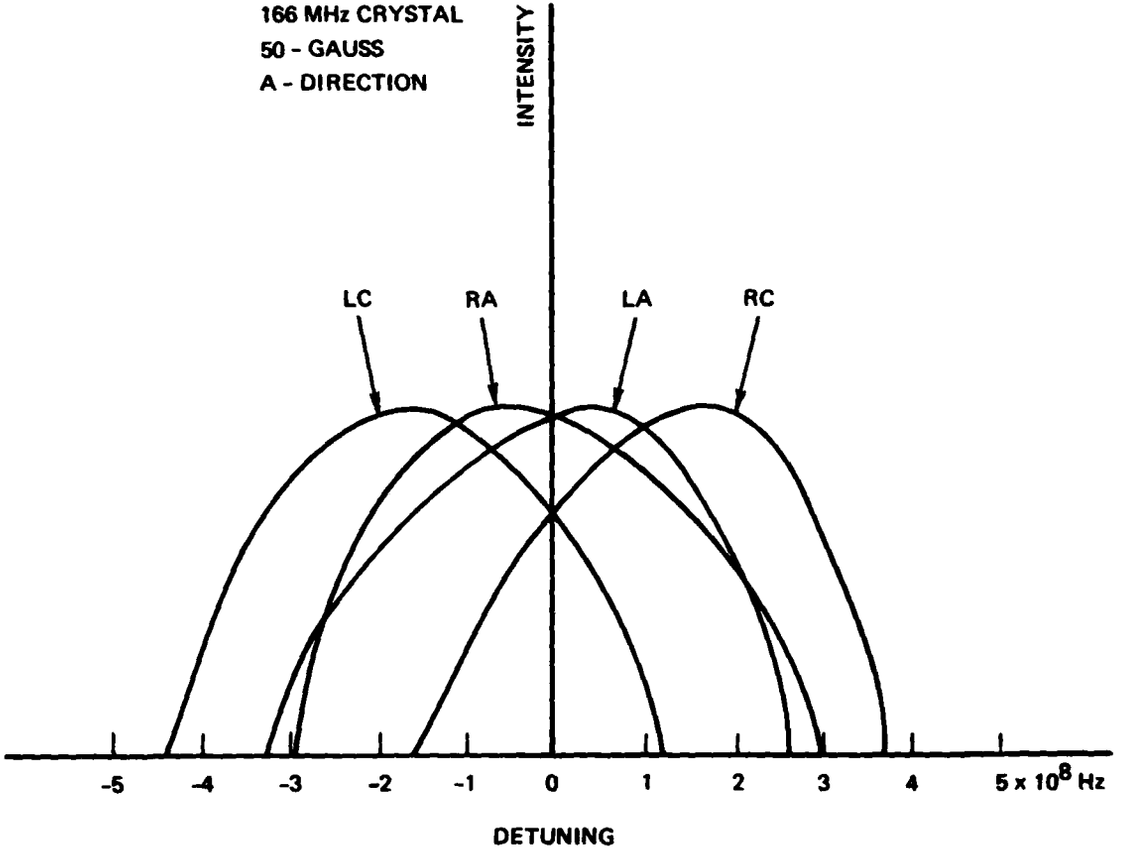

Figure 5g. Intensity versus Cavity Length Tuning

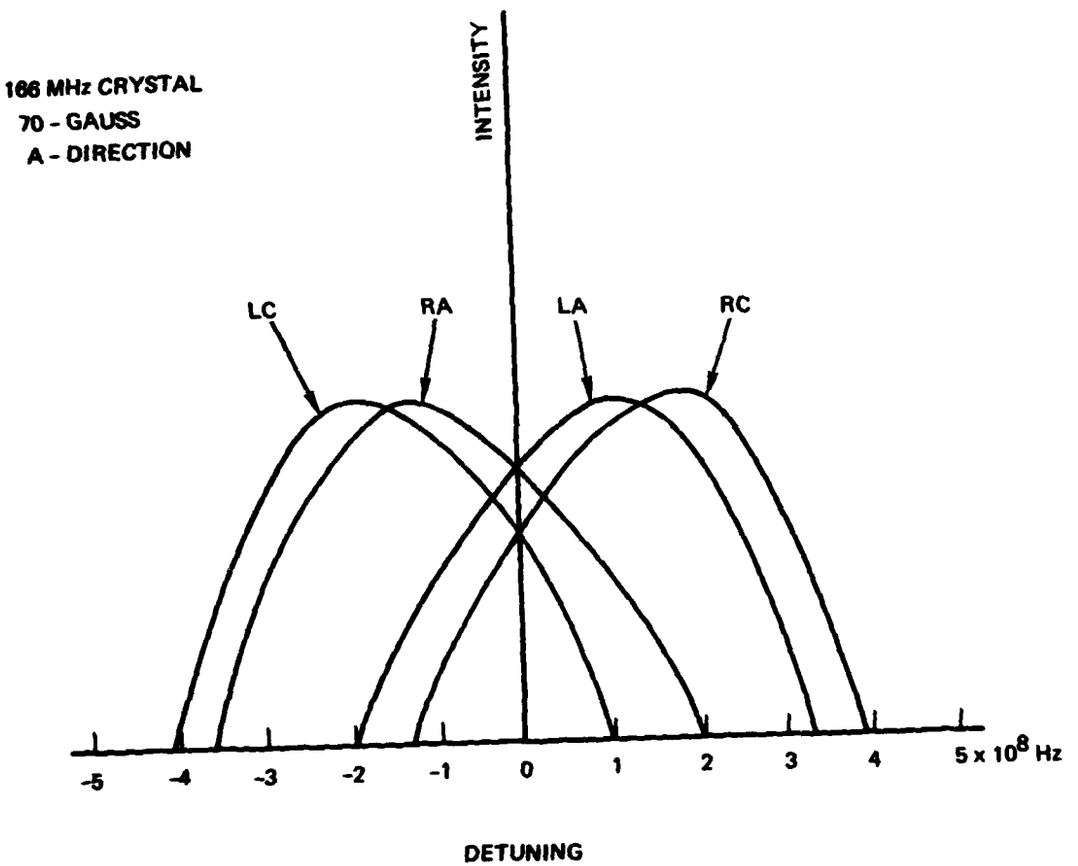

Figure 5h. Intensity versus Cavity Length Tuning

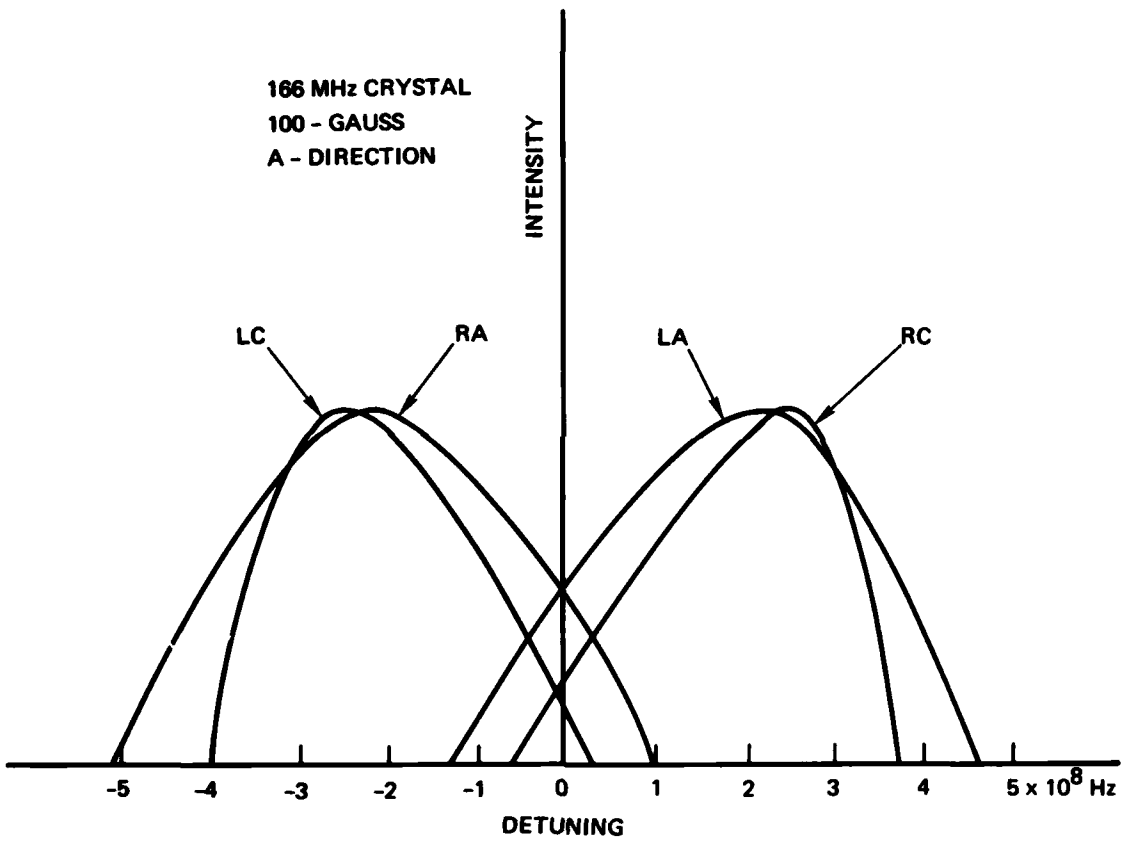

Figure 5i. Intensity versus Cavity Length Tuning

2. Intensity Figures

The curves in figures 6a and b are associated with the 30 MHz crystal:

a. Figure 6a is associated with 40 gauss in the C direction on the plasma. Note that the asymmetry about the peak of each curve is more pronounced than any of those in figures 6a-i.

b. Figure 6b is associated with 80 gauss in the C direction on the plasma.

3. Intensity Figures

The curves in figures 7a-c are associated with 440 MHz crystal:

a. Figure 7a indicates all four oscillating modes to have the same gain profile with zero magnetic field on the dual isotope plasma.

b. Figure 7b indicates the effect of 60 gauss in the C direction on the gain media.

c. Figure 7c indicates the effect of 100 gauss in the C direction on the gain media.

There are several significant comparative features in these curves: Note, the degree of asymmetry in the curves when the magnetic field is applied is significantly less with the 440 MHz crystal than with the other crystals. Note, all four modes in figure 7a have the same gain profile with the 440 MHz crystal as compared to the no field case with the 166 MHz crystal in figure 5a. These two features indicate considerable mode gain competition for the shorter crystals.

The initial comparisons of the data represented in figures (5) through (7) with the theory/model predictions showed the same results with respect to the relations between peak intensity, detuning, and magnetic field but did not indicate the substantial

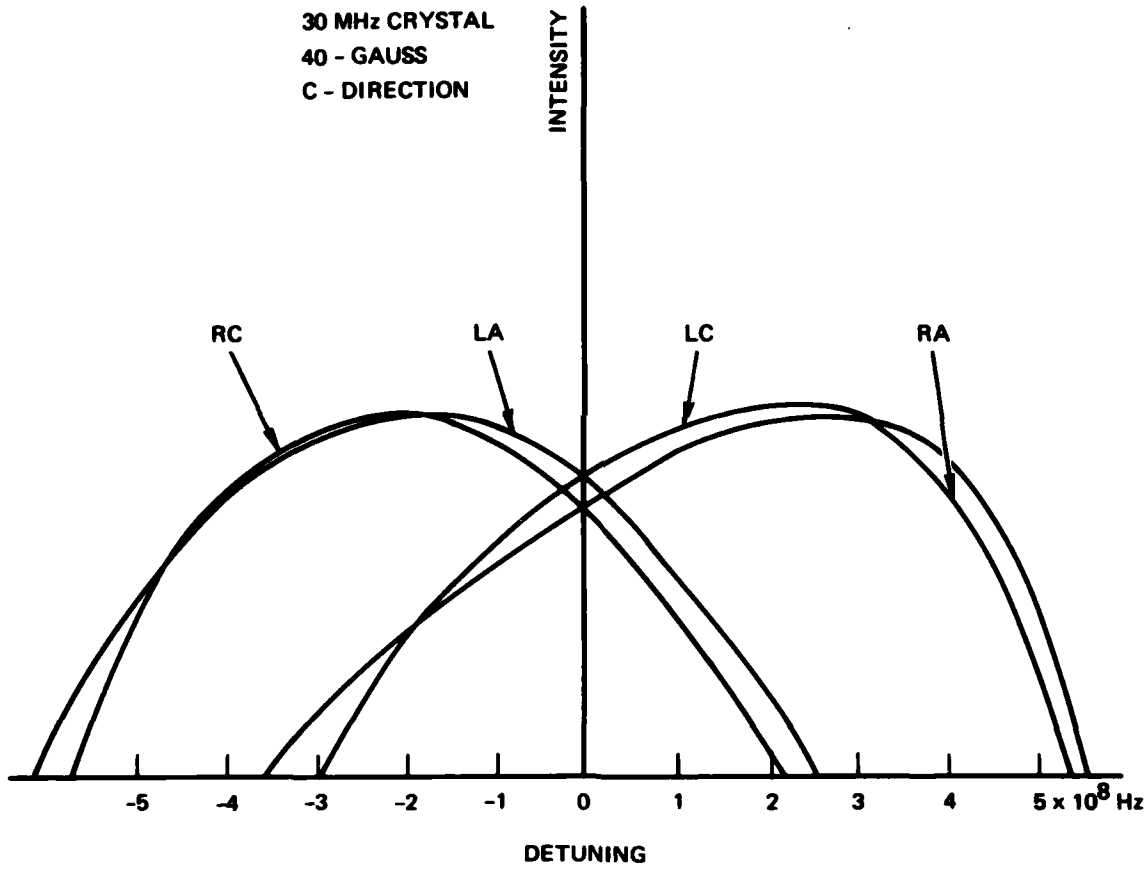

Figure 6a. Intensity versus Cavity Length Tuning

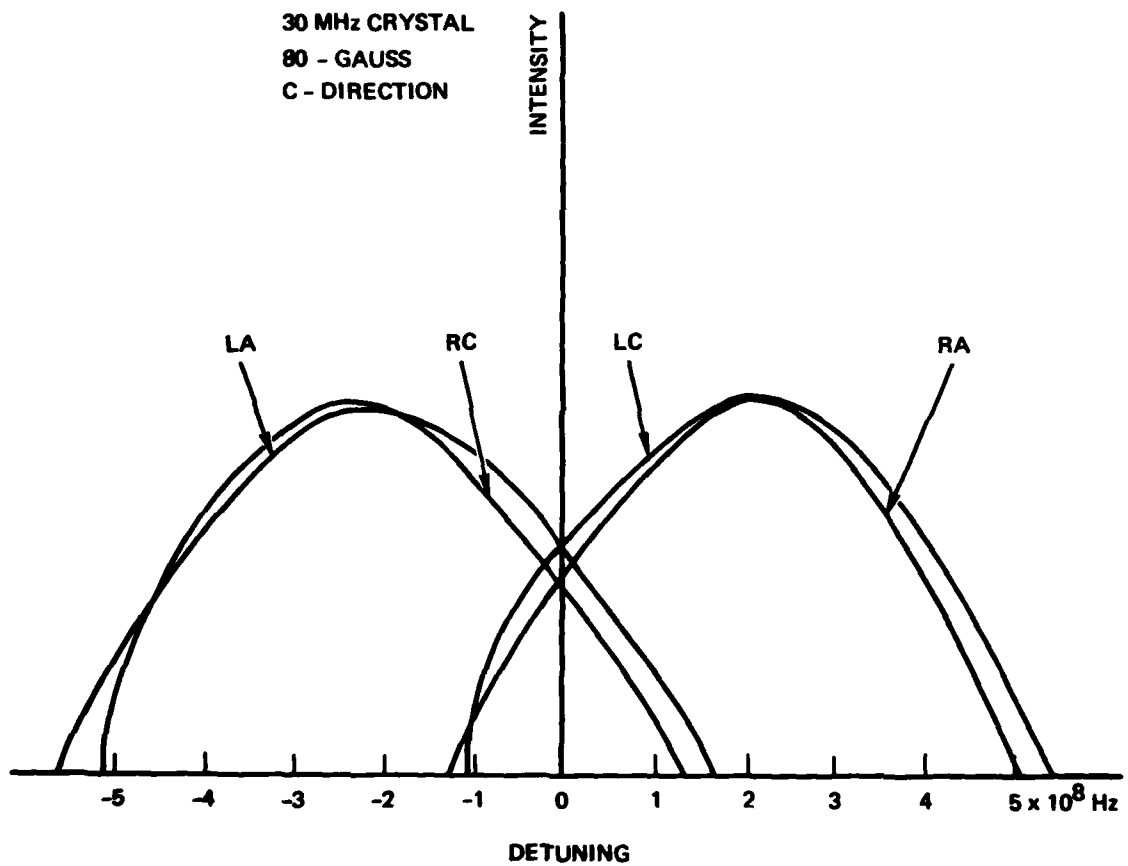

Figure 6b. Intensity versus Cavity Length Tuning

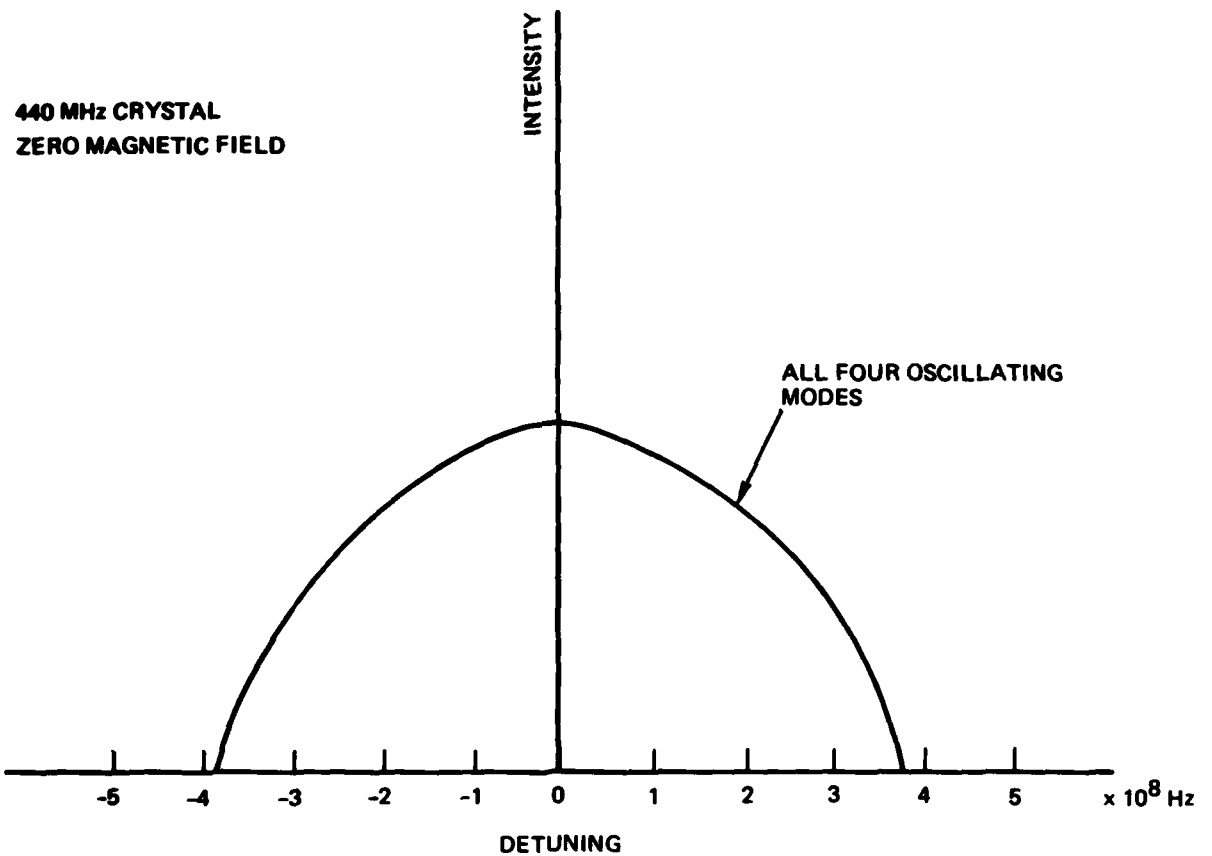

Figure 7a. Intensity versus Cavity Length Tuning

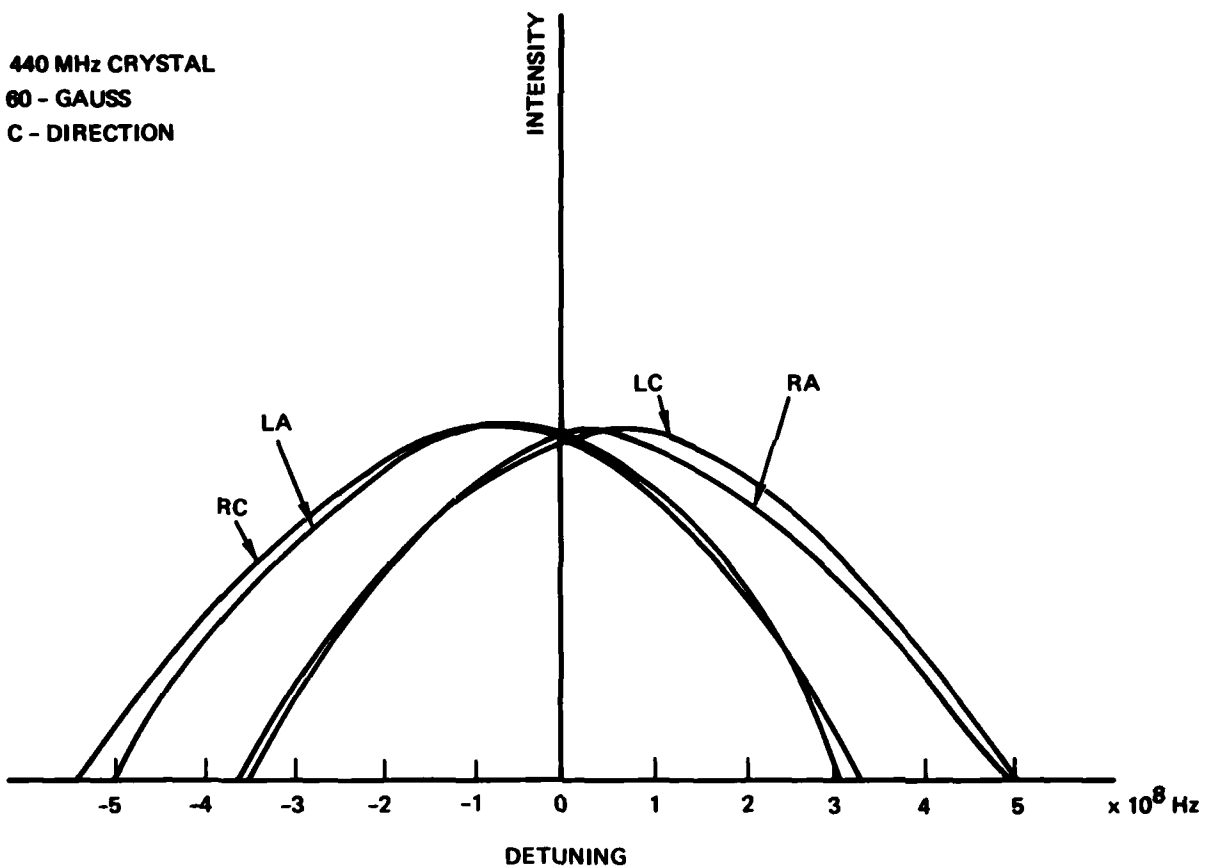

Figure 7b. Intensity versus Cavity Length Tuning

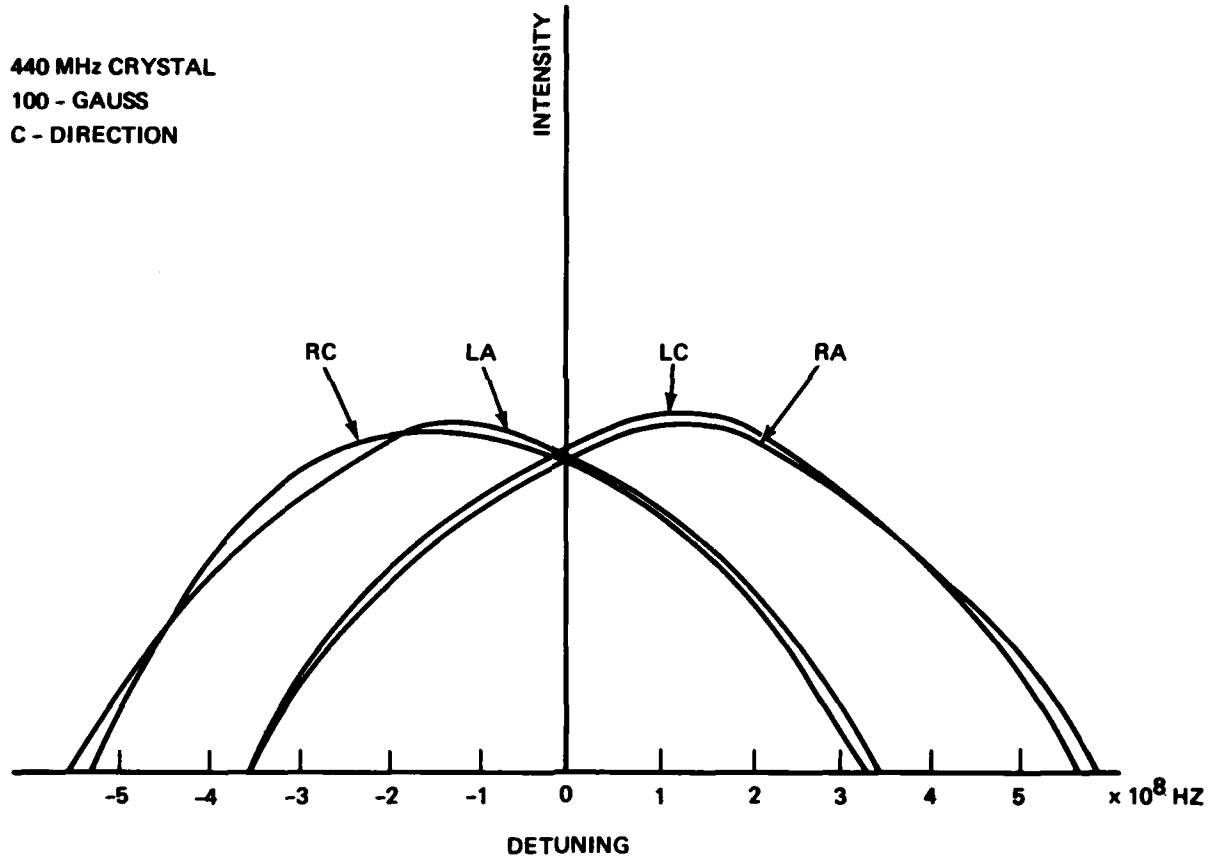

Figure 7c. Intensity versus Cavity Length Tuning

asymmetries shown in the experimental data. However, by an alteration/addition to the early model, which effectively eliminated the "strong Doppler limit" assumption, the later curves generated by the model matched almost identically the experimental curves.

B. $\dot{\psi}$ BEAT NOTE

The following data concerns the $\dot{\psi}$ multioscillator gyro beat-note as defined in equation 3:

$$\dot{\psi} \equiv f_4 - f_3 - f_2 + f_1$$

These measurements were obtained with the ring laser instrument fixed to the gas fill station. Therefore, there is only a small constant (approximately 10 Hz) contribution to $\dot{\psi}$ from the instrument rotating at earth rate. Thus, any variation in $\dot{\psi}$ is substantially a function of the active coupling of the various oscillating modes. In each case, $\dot{\psi}$ is plotted as a function of cavity length detuning for the various indicated axial magnetic fields on the gas plasma. Zero detuning was determined in each case by adjusting the cavity length to a point such that the peak intensity magnitude of the beat-note from the left circular gyro equals that from the right circular gyro. This point is different in absolute frequency space for each of the curves because of the asymmetry in the intensity profiles as a function of magnetic field and because of the different isotope ratios used in the various experiments. (Note the intensity data in figure 5.) Nevertheless, in each case zero detuning of the mean optical frequency is near the midpoint of the 6328Å natural transition frequency associated with the two isotopes Ne^{20} and Ne^{22}.

The crystal frequency splitting being used is indicated on each figure, as is the Ne^{20}/Ne^{22} ratio. The Faraday splitting between (f_4 and f_3) and (f_2 and f_1) may be determined from the indicated magnetic field strength and the data in figure 4. The He/Ne gas ratio was 12/1 in each case. The total gas pressure in each case was 3.0 Torr unless otherwise indicated on the figure. The gain to loss ratio in each case was determined by the plasma current at lasing threshold and was approximately 1.5 unless otherwise indicated. The accuracy of the data points is indicated by the size of the points. The beat-note frequency was determined with an oscilloscope and the detuning by the output from the optical spectrum analyzer on this same oscilloscope.

a. Figures 8a-d demonstrate several $\dot{\psi}$ sensitivities associated with the 166 MHz crystal: Note that in each case a reversal of the direction of the magnetic field causes the slope of the curve to reverse sign and the magnitude of the $\dot{\psi}$ bias (deviation from $\dot{\psi} = 0$) to reverse sign. Furthermore, note that the $\dot{\psi}$ bias may be adjusted to zero by a proper selection of the Ne^{20}/Ne^{22} isotope ratio (see figure 8c) and that variation in the isotope ratio does not significantly change the slopes of these curves. These same features were found to be similar with respect to each of the four crystals.

b. Figures 9a-c demonstrate a $\dot{\psi}$ sensitivity to the gain/loss ratio. This gain/loss ratio was determined by the plasma current ratio at lasing threshold and at the current for which the data was taken. Note that there is no significant difference in figures 9a and 9b. However, the slopes of these curves begin to change as the gain/loss ratio exceeds 2.0. Again, the same was observed for the other crystals: little change in the slopes of these curves until the gain/loss ratio exceeded 2.0.

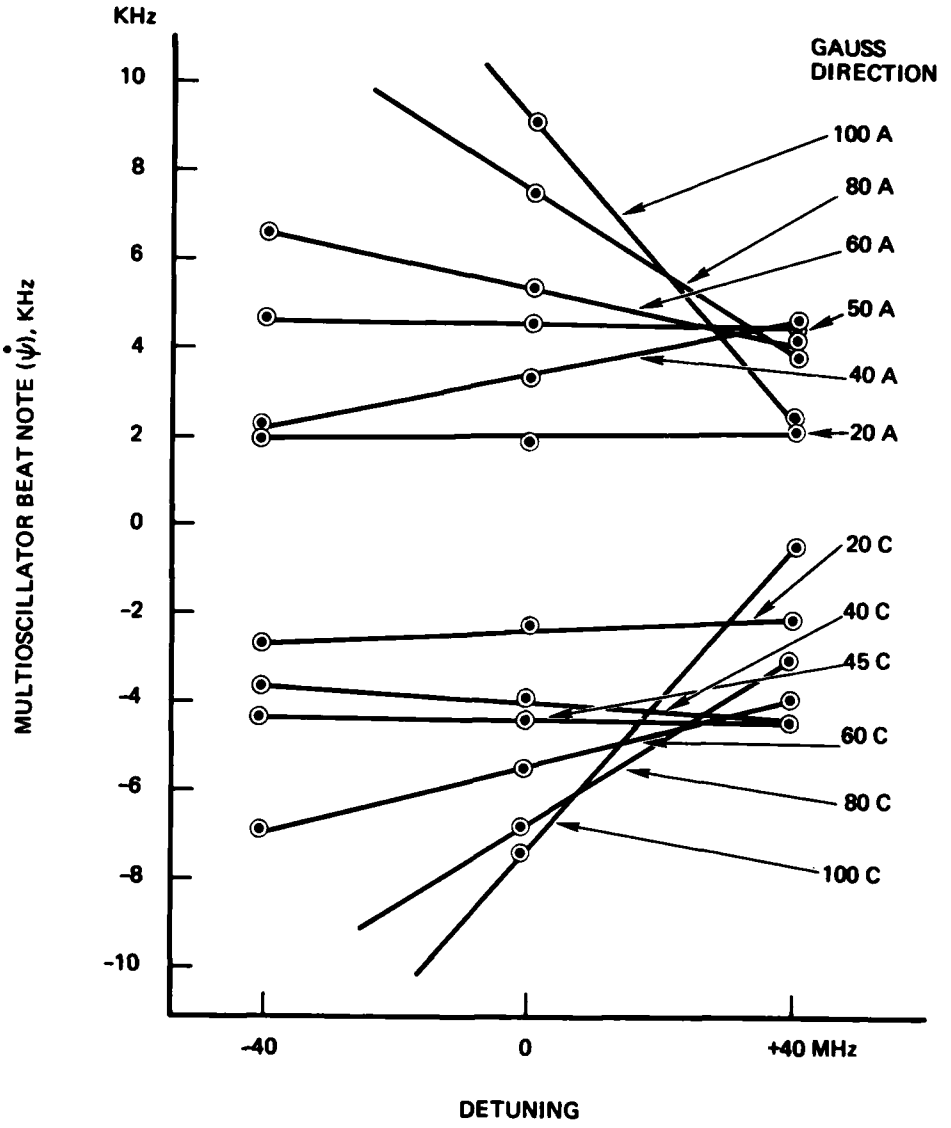

Figure 8a. $\dot{\psi}$ versus Cavity Length Tuning in a Zeeman Multioscillator

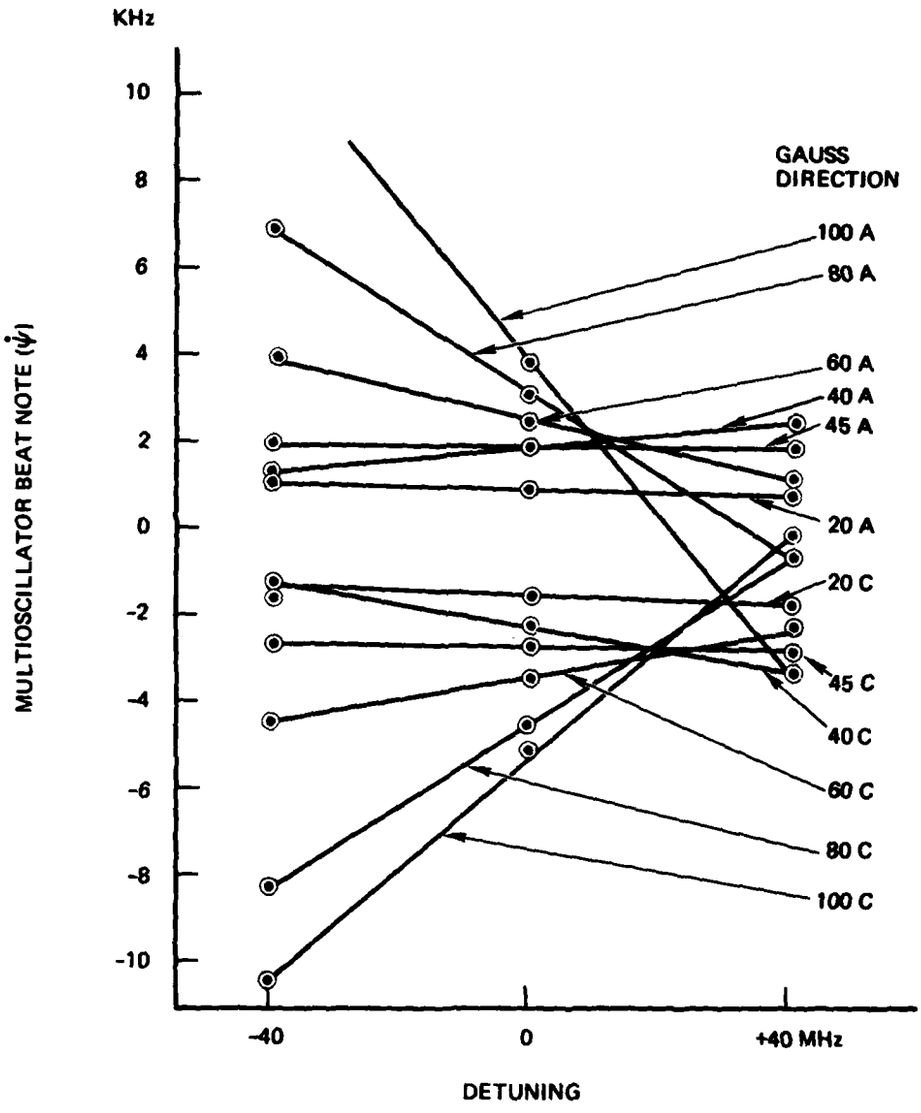

Figure 8b. $\dot{\psi}$ versus Cavity Length Tuning in a Zeeman Multioscillator

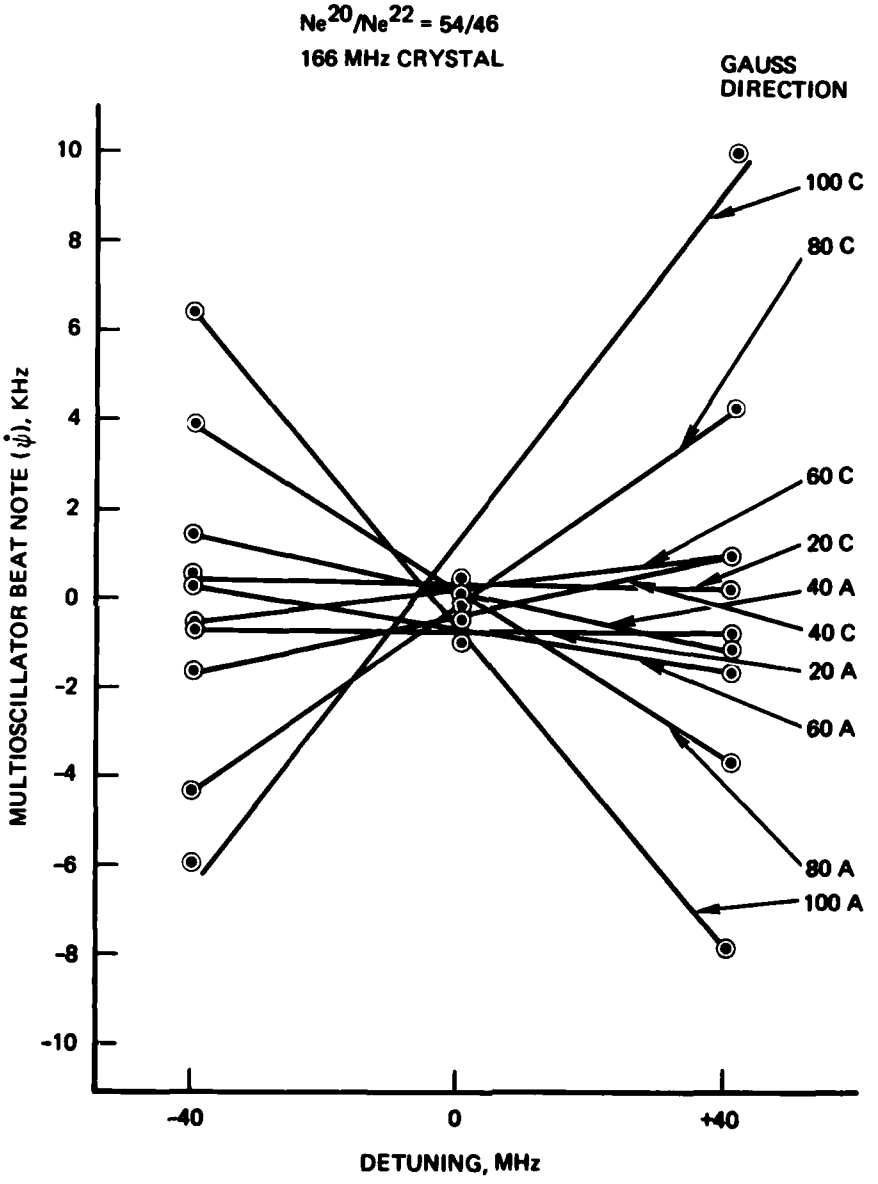

Figure 8c. $\dot{\psi}$ versus Cavity Length Tuning in a Zeeman Multioscillator

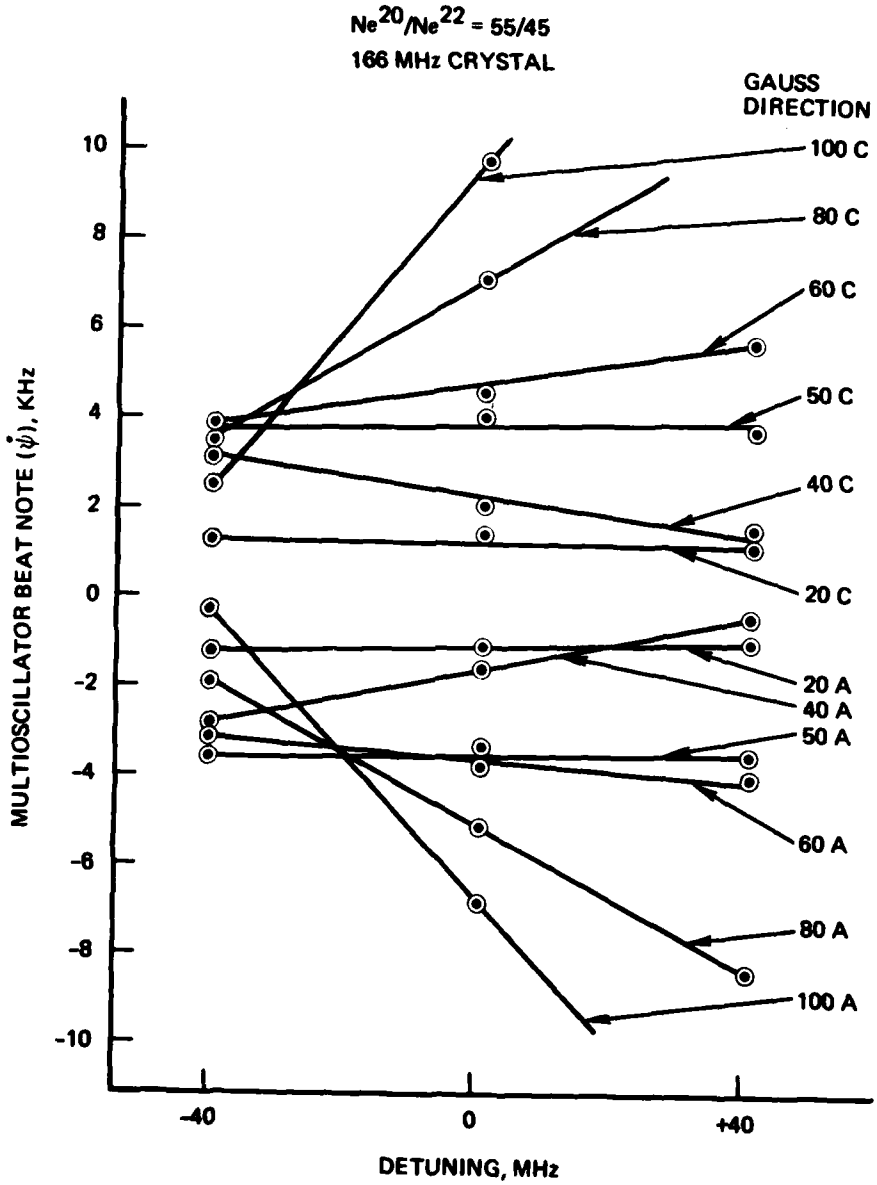

Figure 8d. $\dot{\psi}$ versus Cavity Length Tuning in a Zeeman Multioscillator

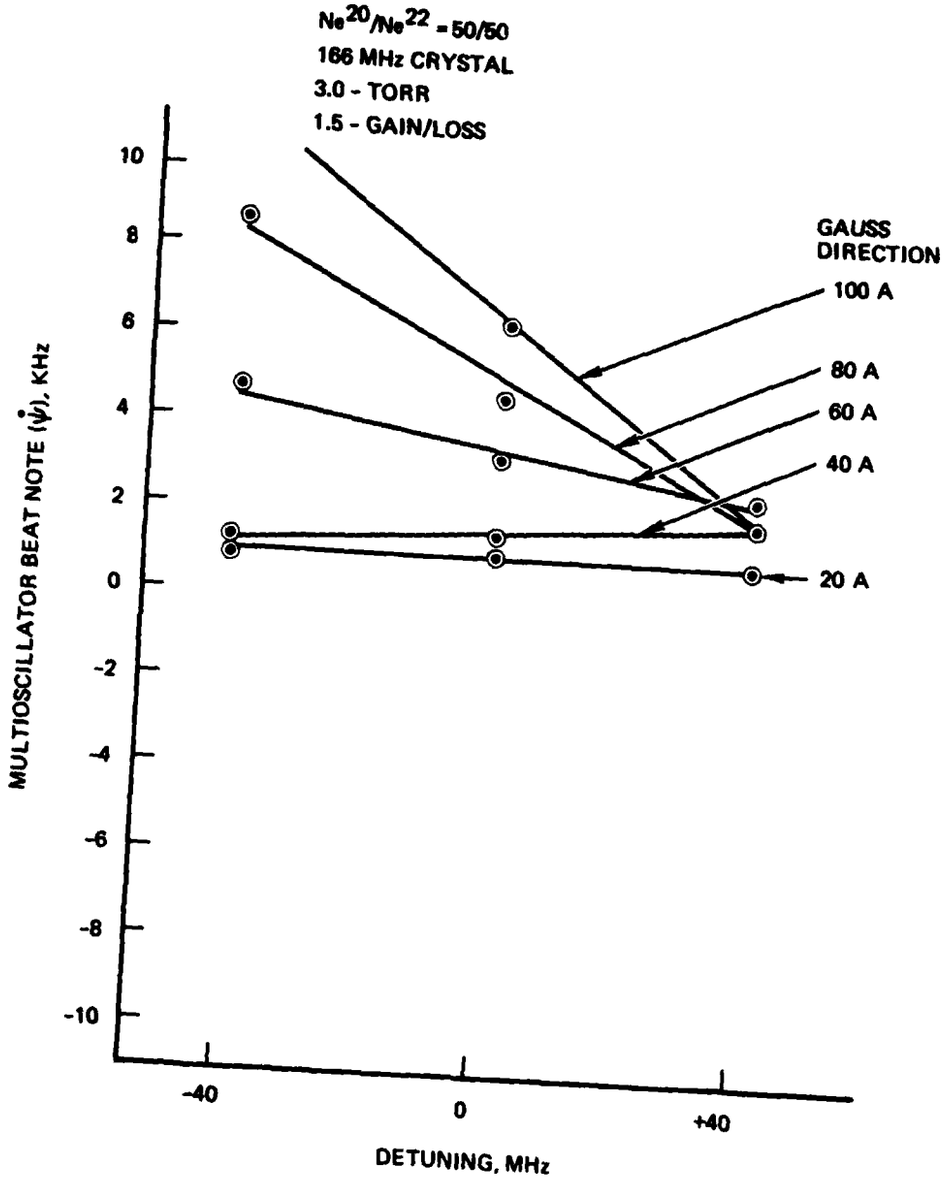

Figure 9a. $\dot{\psi}$ versus Cavity Length Tuning in a Zeeman Multioscillator

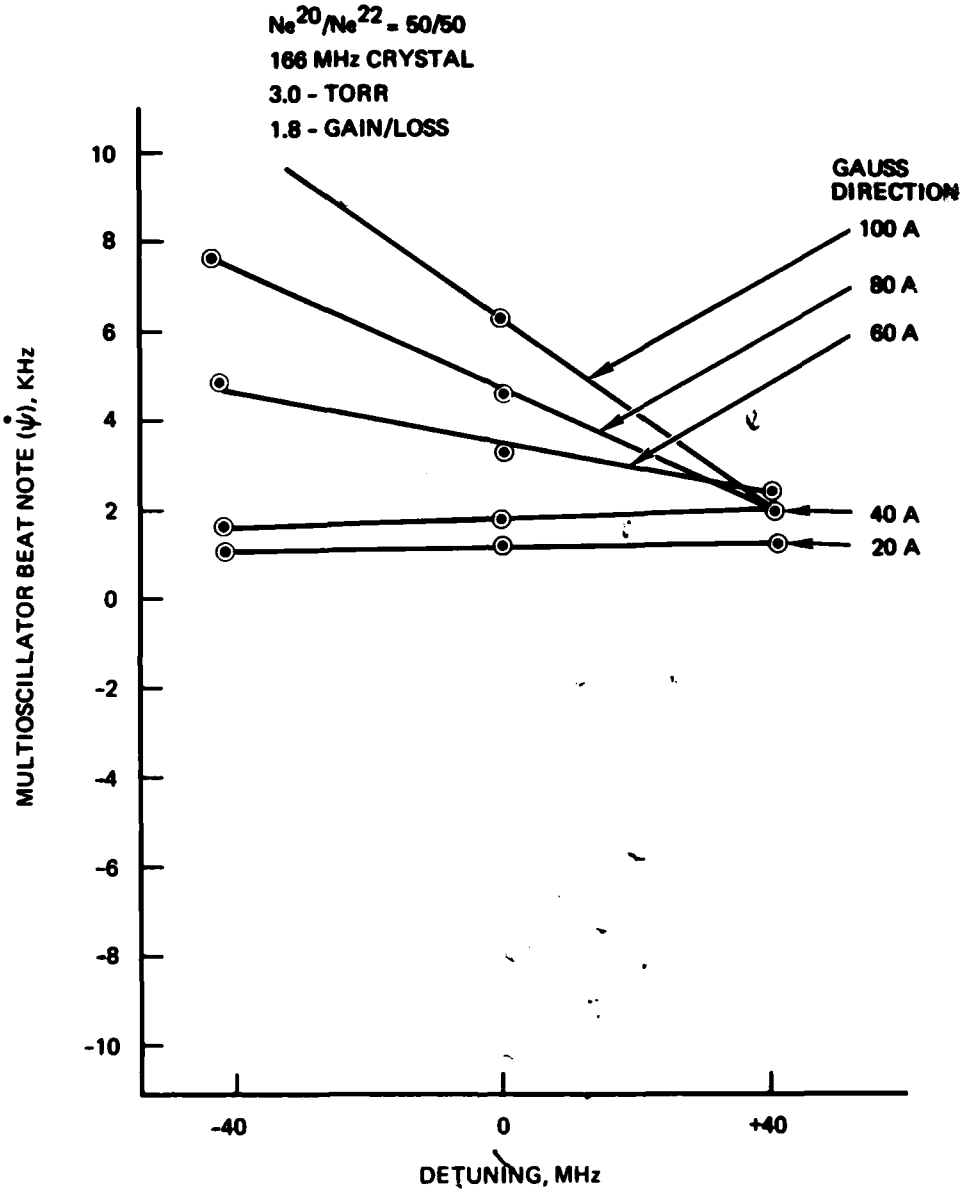

Figure 9b. $\dot{\psi}$ versus Cavity Length Tuning in a Zeeman Multioscillator

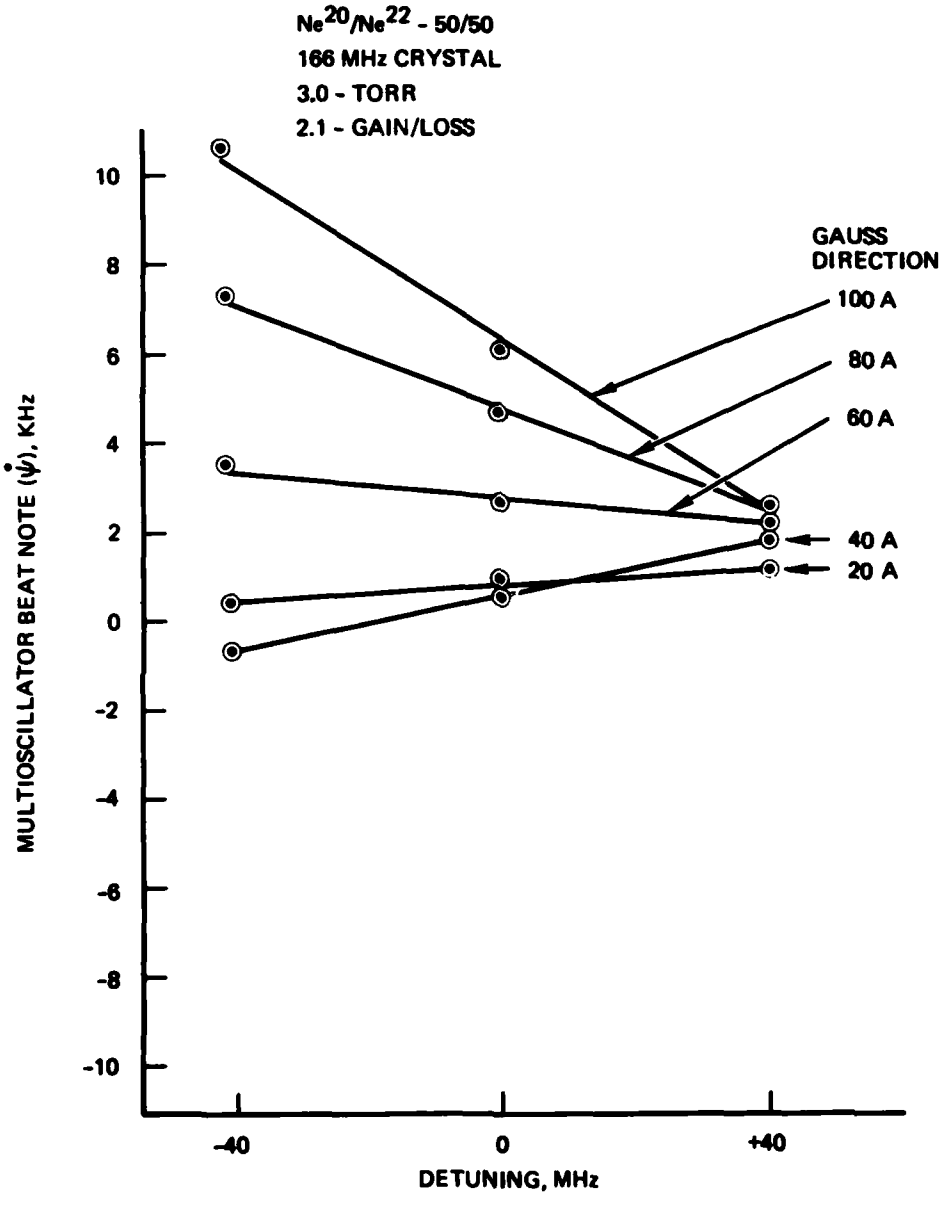

Figure 9c. $\dot{\psi}$ versus Cavity Length Tuning in a Zeeman Multioscillator

c. Figures 10a, 10b, and 9b indicate a $\dot{\psi}$ sensitivity to total gas pressure. These three figures are associated with the 166 MHz crstal. However, all four crystals showed similar results in that the higher pressures had less detuning sensitivity. This particular general result agrees with theory/model predictions.

d. Figures 11a and 11b are associated with the 63 MHz crystal. Again, this data demonstrates the decreased detuning sensitivity with an increase in total gas pressure.

e. Figures 12a and 12b are associated with the 440 MHz crystal. These two figures demonstrate the detuning $\dot{\psi}$ sensitivity and the $\dot{\psi}$ bias sensitivity to isotope ratio.

f. Figures 13a and 13b demonstrate the $\dot{\psi}$ detuning sensitivity associated with the 30 MHz crystal. Again, note the decrease in sensitivity with the increased total pressure.

g. Figure 14 is a compendium of the $\dot{\psi}$ sensitivity experimental data compared with theoretical predictions. The form of this data is different from that in the previous figures. In this case the vertical scale is $\dot{\psi}$/detuning and the horizontal scale represents the magnetic field on the gas gain plasma. All four crystals are represented in this figure. The other laser gyro parameters such as total gas pressure, gain/loss ratio, Ne^{20}/Ne^{22} ratio, etc., were held constant and the same for each crystal in this comparison. The corresponding

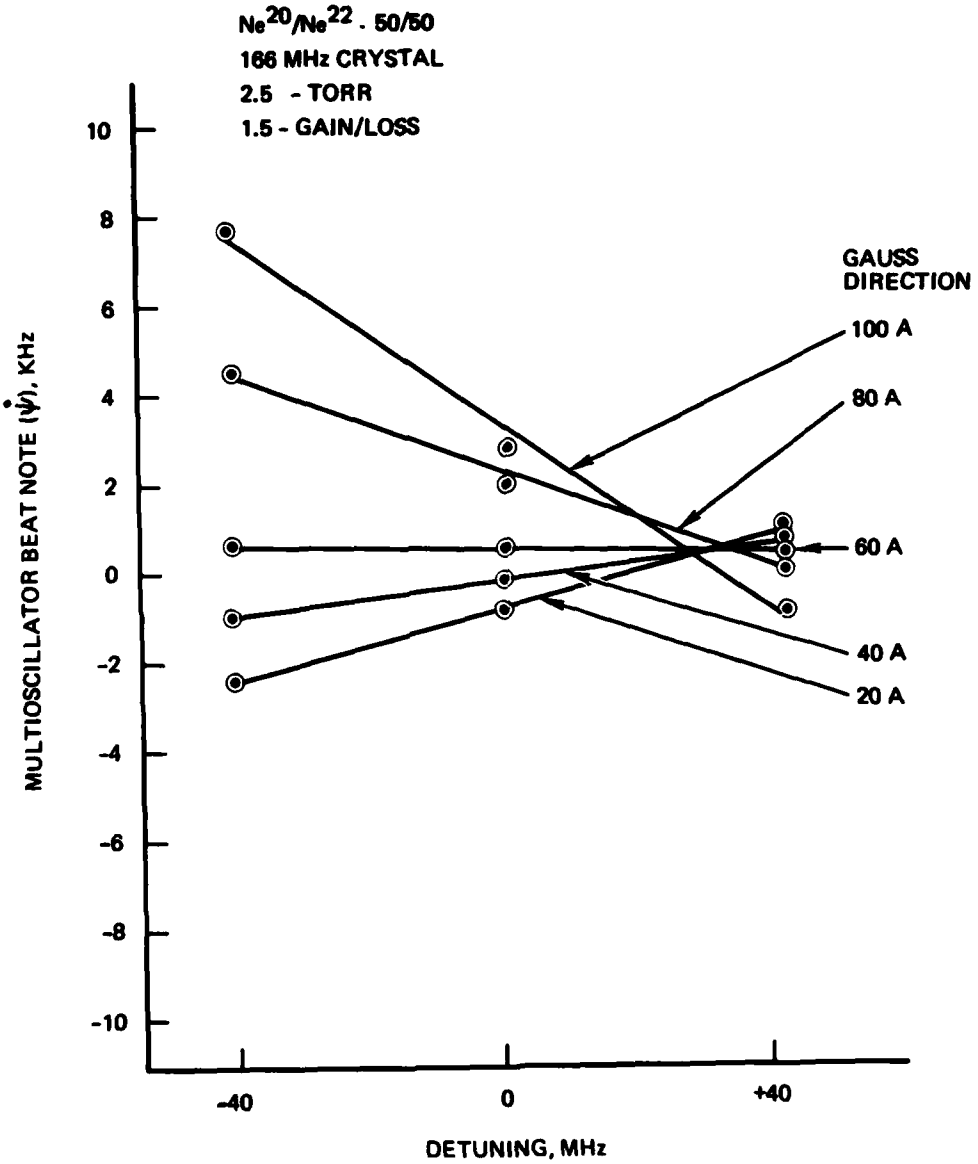

Figure 10a. $\dot{\psi}$ versus Cavity Length Tuning in a Zeeman Multioscillator

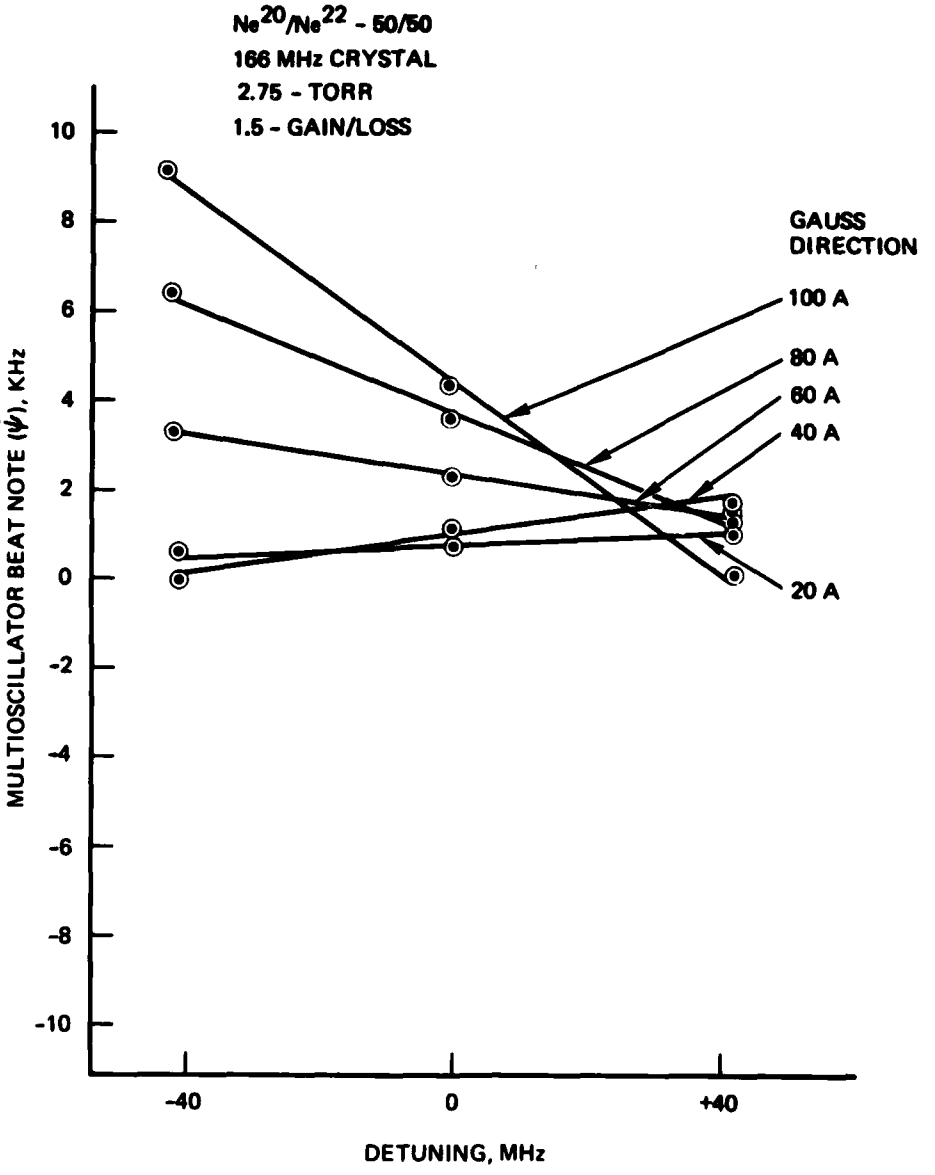

Figure 10b. $\dot{\psi}$ versus Cavity Length Tuning in a Zeeman Multioscillator

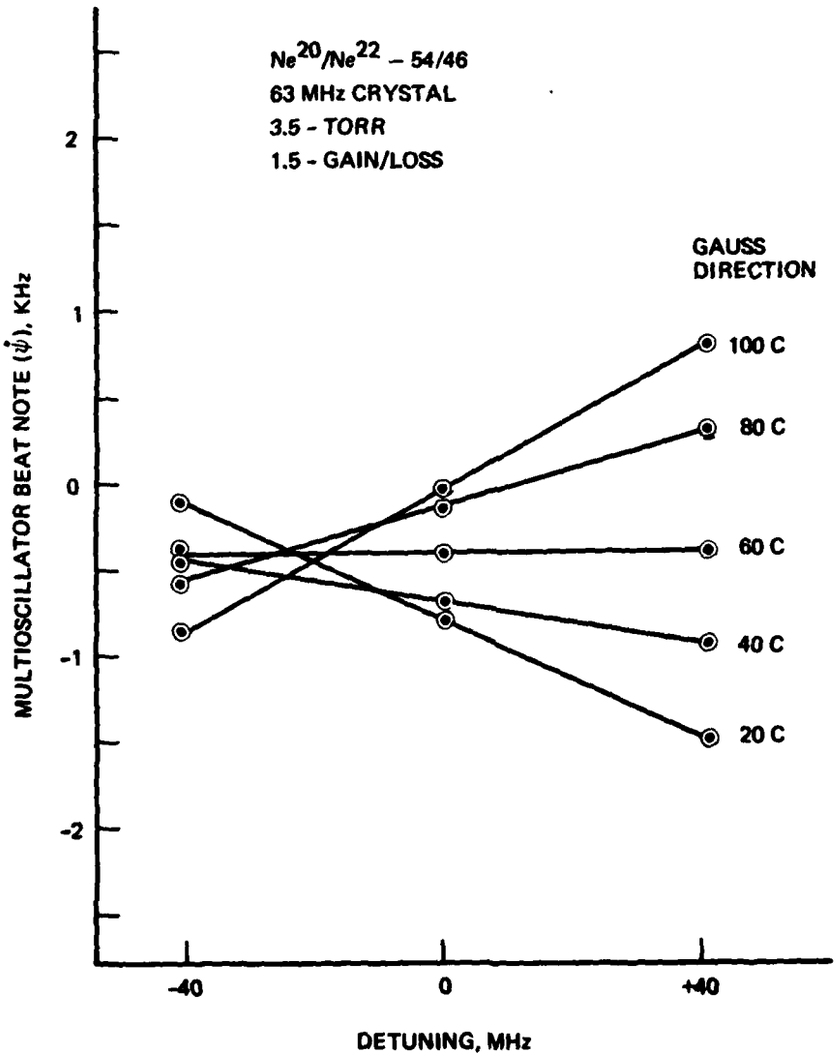

Figure 11a. $\dot{\psi}$ versus Cavity Length Tuning in a Zeeman Multioscillator

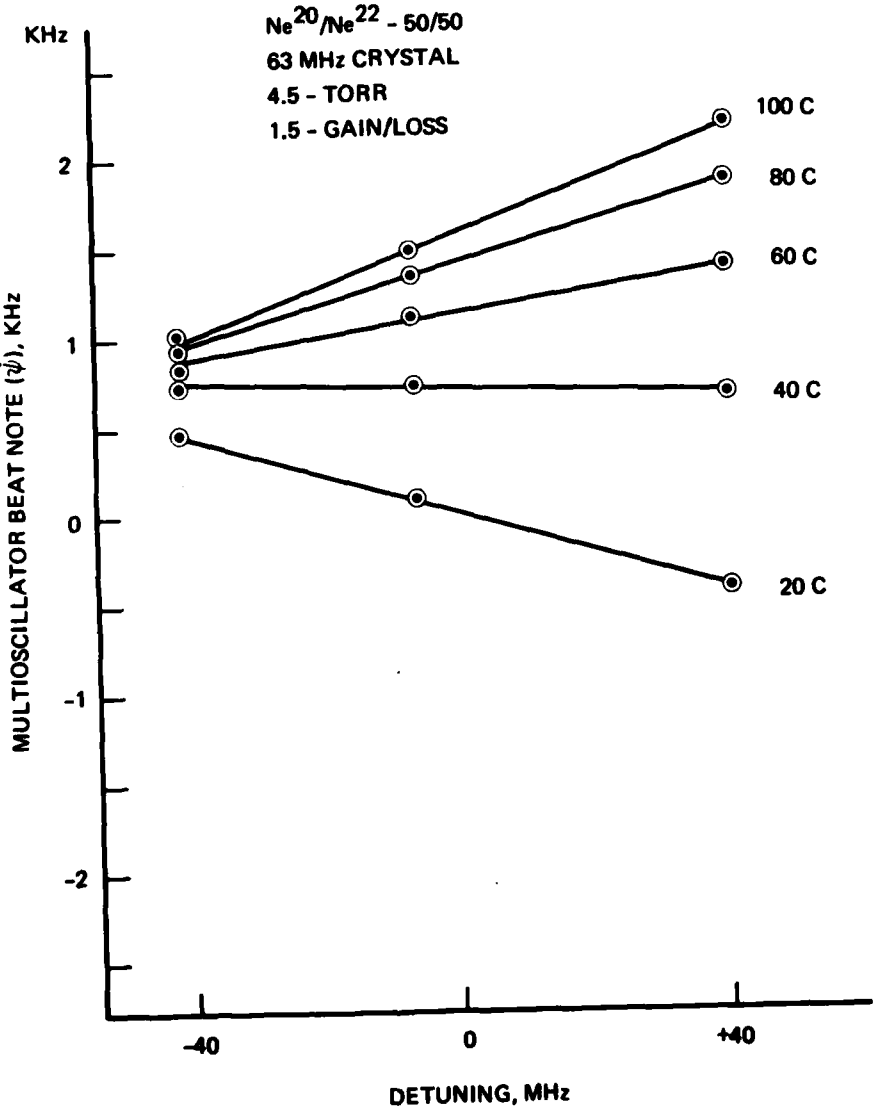

Figure 11b. $\dot{\psi}$ versus Cavity Length Tuning in a Zeeman Multioscillator

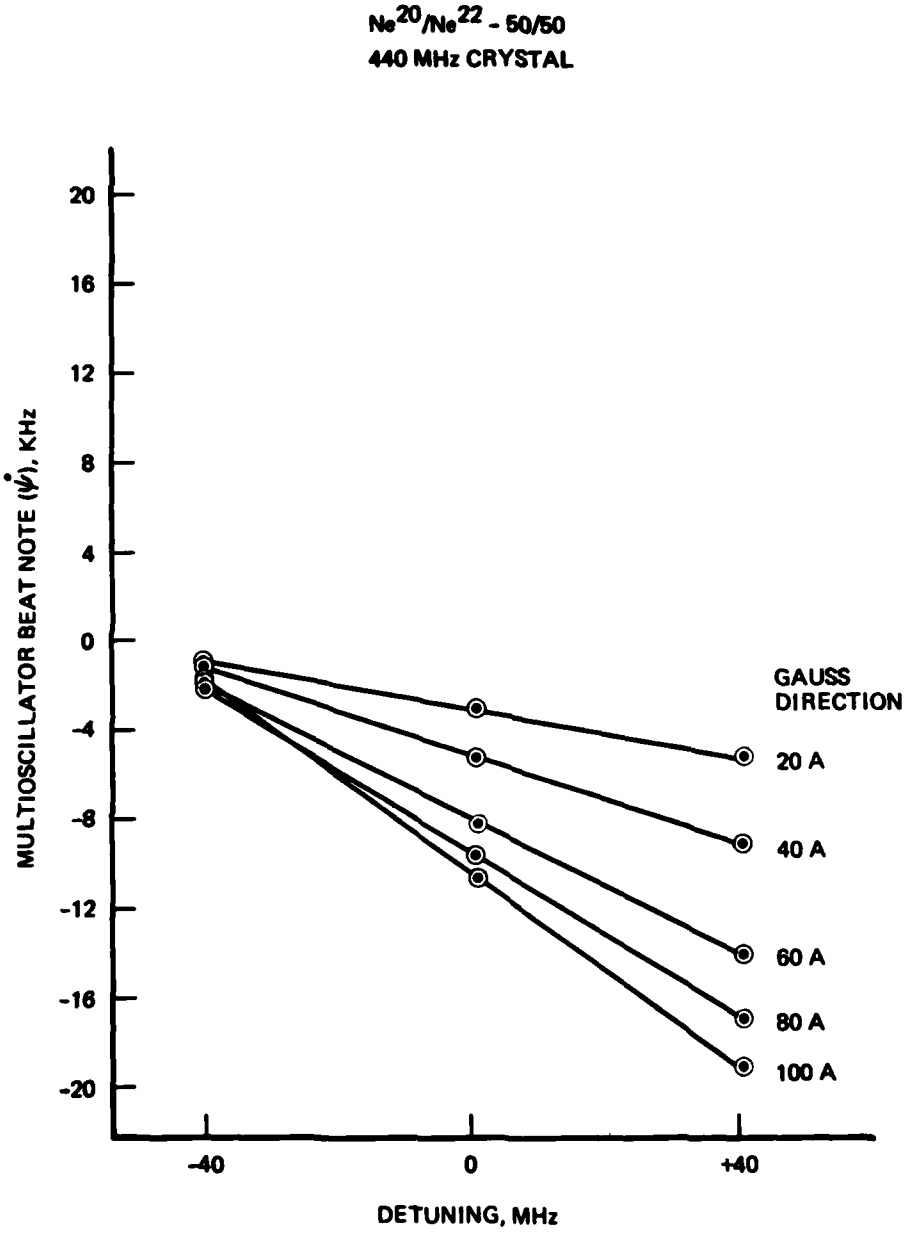

Figure 12a. $\dot{\psi}$ versus Cavity Length Tuning in a Zeeman Multioscillator

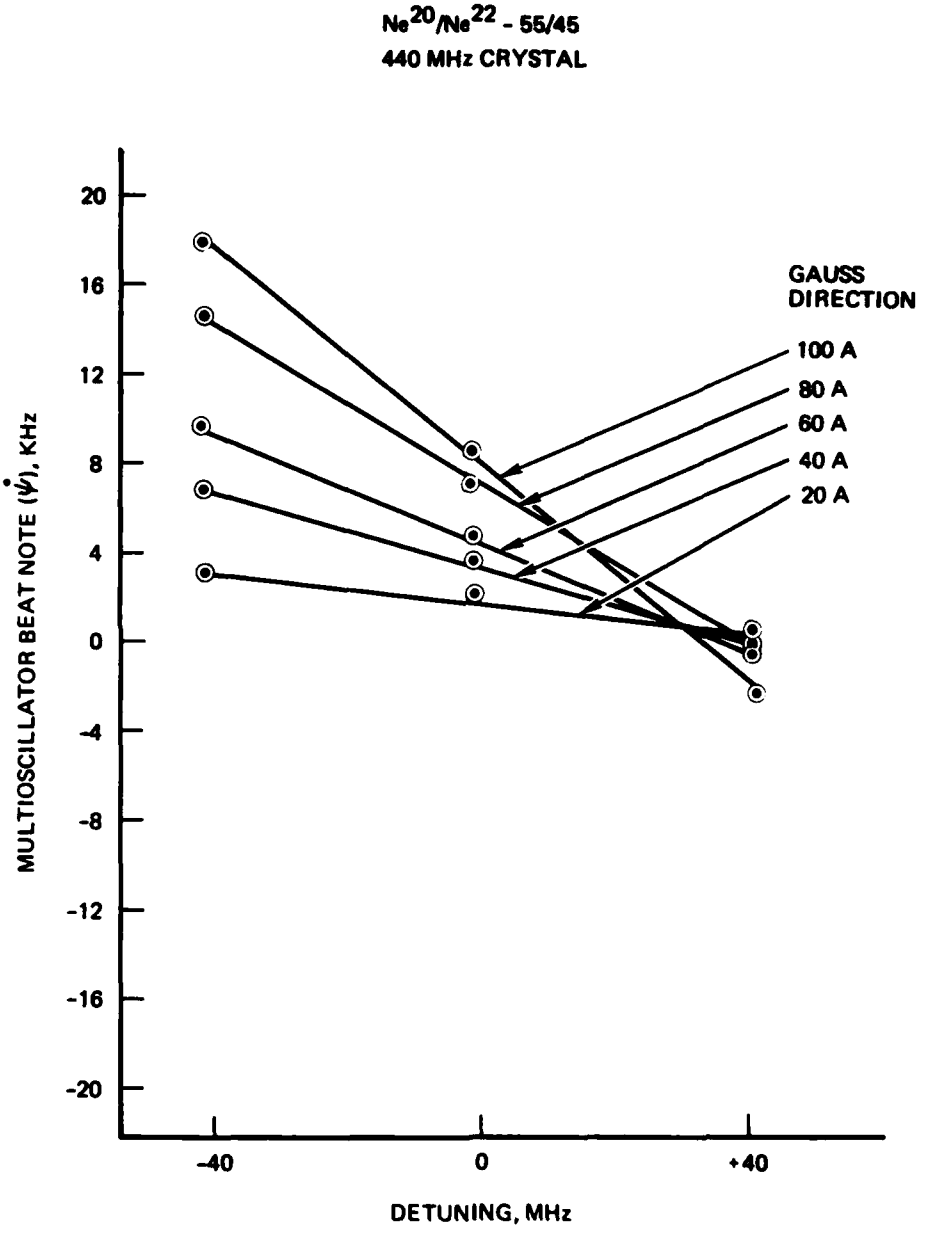

Figure 12b. $\dot{\psi}$ versus Cavity Length Tuning in a Zeeman Multioscillator

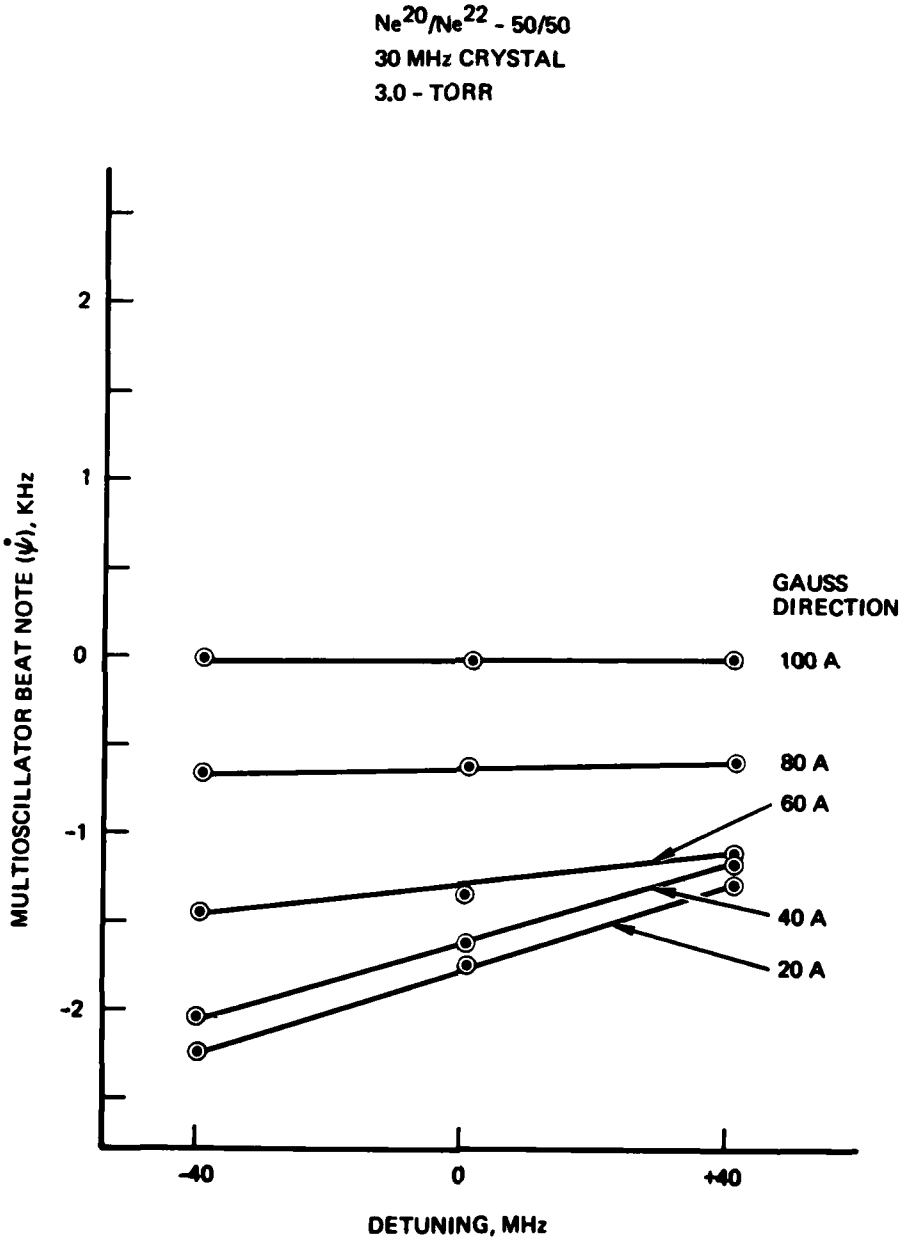

Figure 13a. $\dot{\psi}$ versus Cavity Length Tuning in a Zeeman Multioscillator

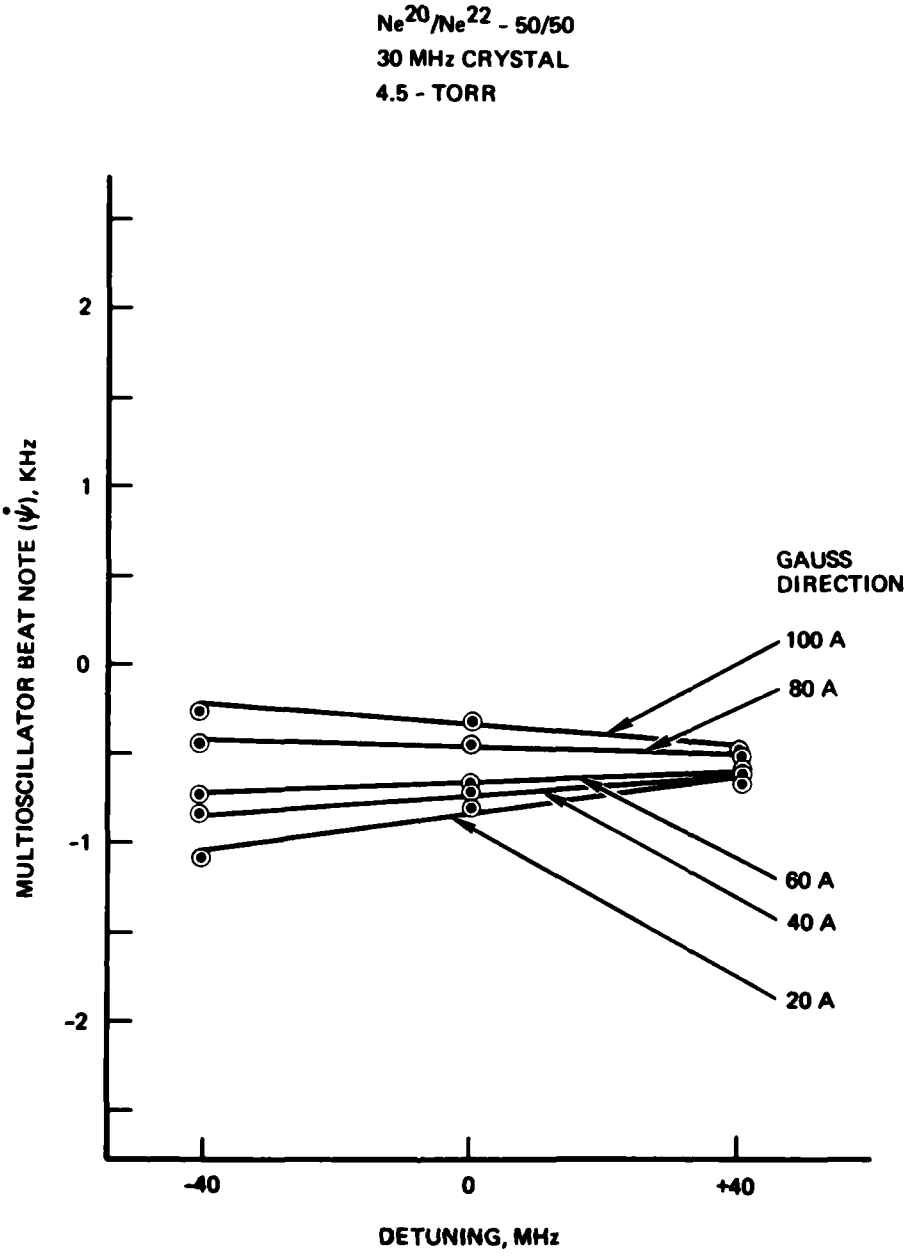

Figure 13b. $\dot{\psi}$ versus Cavity Length Tuning in a Zeeman Multioscillator

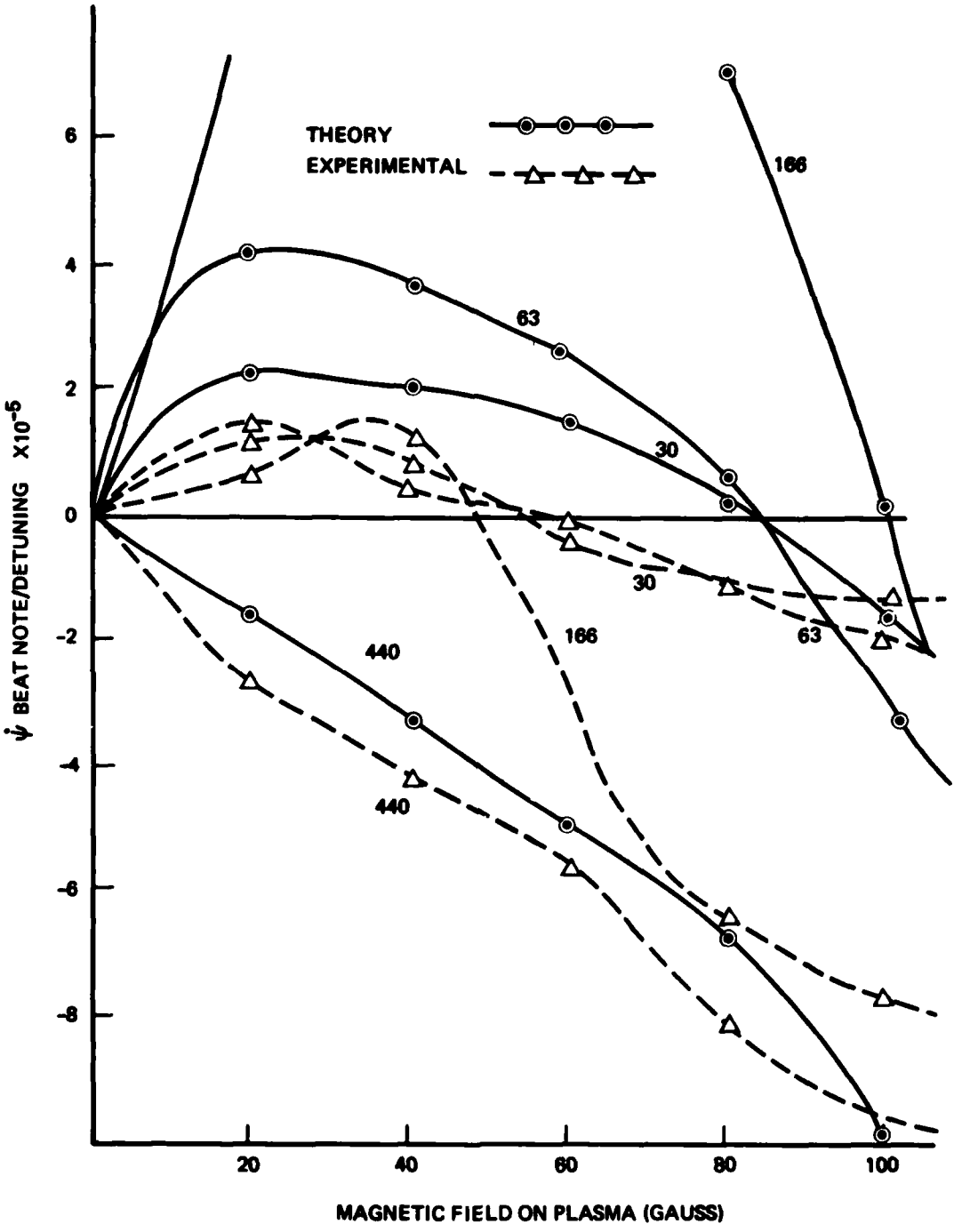

Figure 14. $\dot{\psi}$-Detuning Sensitivity to Magnetic Field in a Zeeman Multioscillator

theoretical constants representing these gyro parameters, such as gas pressure, were chosen to match the experimental parameters as close as possible.

SECTION V
CONCLUSIONS AND RECOMMENDATIONS

There are several cases related herein which may be pointed to as examples of the usefulness of this kind of study in the development of a theoretical model. For example, the degree of asymmetry in the intensity versus detuning curves as a function of magnetic field on the plasma was not known. In this case, the experimental data revealed a need to modify the theoretical assumptions concerning the "strong Doppler limit."

It is significant to note the theory-experiment correlation attained with respect to the $\dot{\psi}$ difference-frequency beat-note data. The comparison in figure 14 shows good agreement between theory and experiment for the long and the short (440 and 30 MHz) crystals. The other two crystals agree within the same order of magnitude with the theory which none of the four did at the beginning of this study.

A continued correlation effort is necessary to continue the refinement of the theory. The $\dot{\psi}$ beat-note parameter sensitivities are of critical importance in designing a Zeeman multioscillator. Much progress has been made during this study period with respect to matching experimental data with the $\dot{\psi}$ calculations. A continued effort is recommended.

REFERENCES

1. H. deLang, "Eigenstates of Polarization in Lasers," Philips Res. Repts. 19, p. 439, 1964.

2. V. E. Sanders and R. M. Kiehn, "Dual-Polarized Ring Lasers," IEEE J. of Quantum Electronics, Vol. QE-13, No. 9, p. 739, Sept. 1977, and G. B. Yntema, D. C. Grant, Jr., and R. T. Warner, "Differential Laser Gyro System," U.S. Patent 386203, Jan. 1975.

3. a. David R. Hanson and Murray Sargent III, "Theory of a Zeeman ring laser: general formalism," Phys. Rev. A 9, 466 (1974).

b. Weng W. Chow, Jarel Hambenne, David R. Hanson, Murray Sargent III, and Marlan O. Scully, "Theory of a Zeeman ring laser; II: special cases," submitted for publication.

4. W. E. Lamb, Jr., "Theory of an Optical Maser," Phys. Rev. 134, A1429 (1964).

APPENDIX A

POLARIZATION CHARACTERISTICS OF AN ANISOTROPIC RING LASER

POLARIZATION CHARACTERISTICS OF AN ANISOTROPIC RING LASER

Virgil E. SANDERS
Litton Guidance and Control Systems, Woodland Hills, CA 91364, USA

Received 11 January 1979

Experimental evidence is presented showing the polarization characteristics of the oscillating modes in an active 6328 Å He–Ne gas ring laser cavity to be determined solely by the anisotropic characteristics of the passive ring cavity. The data is compared to that predicted from a Jones matrix analysis of the passive cavity.

In an anisotropic He–Ne ring laser, it is possible to have simultaneous continuous laser oscillation of two polarization eigenstates of a single transverse mode in each direction. It has been shown [1] that the relative frequencies of these four oscillating eigenstates are substantially a function of the anisotropies in the laser cavity and of the isotropic nonreciprocal phenomena such as rotation of the cavity. This is, of course, not true in the presence of strong active coupling between eigenstates propagating in the same or opposite directions. Two or more of these oscillations may be coupled strong enough such that they oscillate at the same frequency irrespective of the magnitude of the anisotropies or the nonreciprocal phenomena. The data presented herein shows that, in the absence of strong coupling between two modes propagating in the same direction, the electric field polarization states of these eigenstates are completely determined by the anisotropies in the passive ring cavity.

The ring laser apparatus used in this equipment was constructed from a solid block of CerVit. The block has machined clearance holes, gain bores, and aperture to accommodate both the optical and electrical discharge paths. Both the mirrors and electrodes were affixed to polished surfaces on the solid block. The closed optical path of this ring laser is approximately 32 centimeters long. The CerVit block has two separate 4 centimeter long equal gain regions. The electrodes (one cathode and two anodes) were positioned such that the Langmuir flow effects from the plasma gain media flow cancel. The He–Ne gas was an equal mixture of ^{20}Ne and ^{22}Ne with the He:Ne pressure ratio being 13:1 at a total pressure of 3 torr.

A quartz crystal approximately 0.066 centimeters in length (along its rotary axis) was installed in the optical cavity as the only anisotropic element in the cavity. This element establishes an approximate 63 MHz frequency splitting between the modes of opposite circular polarization propagating in the same direction. Thus, coupling between these two modes is significantly reduced. The combined remainder of the passive ring cavity, the mirrors, constitute an equivalent single, almost isotropic element. The measured birefringence phase anisotropy of the ring laser cavity without the crystal was less than 0.05 degrees and the loss, Q, anisotropy was less than 0.0001. The quartz crystal had parallel, polished, anti-reflection coated faces approximately perpendicular to the rotary axis of the crystal. The crystal was installed in the ring cavity in a manner such that it could be rotated, or tilted about an axis parallel to the polished faces and perpendicular to the laser beam axis. If the laser beam axis and the crystal rotary axis are not parallel, the crystal element appears slightly birefringent to the laser beam. Fig. 1 is a graph of the measured phase birefringence as a

This work was supported by the U.S. Air Force Office of Scientific Research and Air Force Avionics Laboratory ASD Contract #33615-78-C-1524.

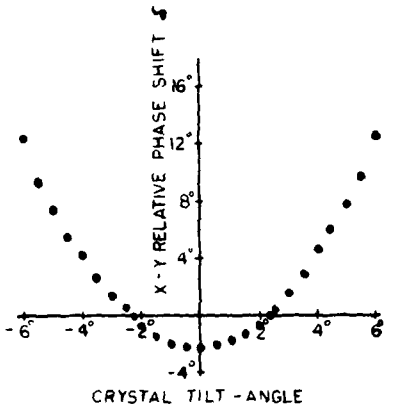

Fig. 1. Crystal tilt-angle versus X-Y phase anisotropy.

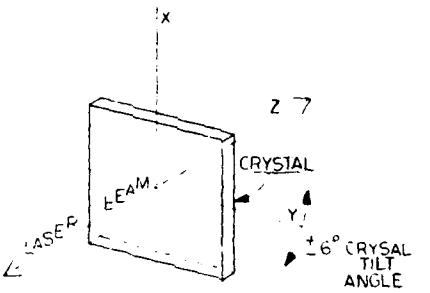

Fig. 2. Coordinates relative to crystal.

function of this crystal tilt-angle. The error in this data is indicated by the size of the dots on the graph. Zero degrees tilt-angle represents the polished faces of the crystal being normal to the laser beam propagating through it. Since the remainder of the ring laser cavity is isotropic, this crystal element defines a pseudo principal cartesian coordinate axis set for the total ring cavity. The X axis we define parallel to the rotation axis of the crystal tilt. With the laser beam path being the Z axis, the Y axis is orthogonal to the X axis and tilts ±6° orthogonal to the Z axis (see fig. 2).

The purpose here is to demonstrate that in a 6328 Å He–Ne ring laser, if the anisotropic characteristics of the passive ring laser cavity are known, one may calculate, via the Jones matrix calculus [2], the expected polarization characteristics of the lasing modes in the active cavity. Each physical element in the ring cavity is represented by a two-by-two matrix. The crystal element in this experiment is both birefringent and a polarization rotator.

A birefringent element is represented by the matrix

$$\begin{pmatrix} \exp(i\delta/2) & 0 \\ 0 & \exp(-i\delta/2) \end{pmatrix},$$

where δ is the relative X-Y phase shift (birefringence) introduced by the element. A polarization rotator is represented by the matrix

$$\begin{pmatrix} \cos\theta & -\sin\theta \\ \sin\theta & \cos\theta \end{pmatrix},$$

where θ is the angle through which an electric vector is rotated by passing through the element. The crystal element in this experiment is represented by the product of these two matrices:

$$\begin{pmatrix} \exp(i\delta/2)\cos\theta & -\exp(i\delta/2)\sin\theta \\ \exp(-i\delta/2)\sin\theta & \exp(-i\delta/2)\cos\theta \end{pmatrix}.$$

In the Jones calculus a two-by-two matrix may be formed which represents the total ring cavity. This matrix is formed by taking the product of the matrices representing the individual cavity elements. The product is taken in the order in which the modes encounter then during a single pass around the cavity. There exist possible electric vector polarization states of these oscillating resonant modes such that a single pass around the cavity does not change this polarization state. This may be represented mathematically by the eigenvalue equation:

$$\boldsymbol{M}\boldsymbol{E}_n = \lambda_n \boldsymbol{E}_n, \tag{1}$$

where $\boldsymbol{M}$ is the Jones matrix representing the total ring cavity, $\boldsymbol{E}_n$ is the single pass regenerative eigenvector field of the nth longitudinal mode, and λ_n represents the eigenvalue single pass phase shift in $\boldsymbol{E}_n$.

In this experiment the ring cavity without the quartz crystal may be represented by the identity matrix

$$\begin{pmatrix} 1 & 0 \\ 0 & 1 \end{pmatrix}.$$

Therefore, with the addition of the crystal element, the matrix $\boldsymbol{M}$, representing the total cavity, becomes

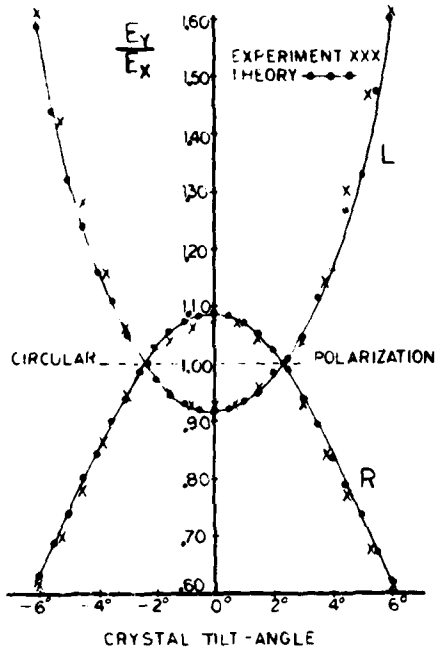

Fig. 3. Crystal tilt-angle versus ellipticity of laser modes.

the same as the matrix representing the crystal element.

$$M = \begin{pmatrix} \exp(i\delta/2)\cos\theta & -\exp(i\delta/2)\sin\theta \\ \exp(-i\delta/2)\sin\theta & \exp(-i\delta/2)\cos\theta \end{pmatrix}.$$

To determine the expected polarization states of the modes in this ring cavity one may solve eq. (1) for the eigenvectors associated with M. The normalized vector are:

$$E_{R,L} = \begin{pmatrix} E_X \\ E_Y \end{pmatrix} = \begin{Bmatrix} \exp(i\delta/2)\sin\theta \\ i\sin\tfrac{1}{2}\delta\cos\theta \pm i[1-(\cos\tfrac{1}{2}\delta\cos\theta)^2]^{1/2} \end{Bmatrix},$$

where the + sign goes with E_R, the right circularly polarized mode, and the − sign goes with E_L, the left circularly polarized mode.

The solid line with the dots in fig. 3 is a plot of the calculated vector magnitude ratio E_Y/E_X for both E_R and E_L as a function of the crystal tilt-angle:

$$\frac{E_Y}{E_X} = \frac{\sin\tfrac{1}{2}\delta\cos\theta \pm [1-(\cos\tfrac{1}{2}\delta\cos\theta)^2]^{1/2}}{-\sin\theta},$$

where the optically active crystal element rotates the electric vector on a single pass through by $\theta = 12.4$ degrees. δ is the relative X-Y phase shift as taken from the measurements recorded in fig. 1. The X's in fig. 3 are the measured field intensity ratio E_Y/E_X from the output of the ring laser as a function of the crystal tilt-angle in the ring laser cavity. Again, the error in this data is approximated by the size of the X's. This data was the same for the two cases: 1) the modes of like polarization and opposite direction strongly coupled and frequency locked, 2) the modes of like polarization and opposite direction weakly coupled and not frequency locked.

In conclusion, in the absence of strong frequency coupling between two active oscillations propagating in the same direction in a four-mode 6328 Å He–Ne ring laser cavity, the polarization state of each resonant mode is solely a function of the anisotropic passive ring cavity. A Jones matrix analysis of the anisotropic passive cavity will substantially determine the polarization characteristics of each generated resonant oscillation.

References

[1] V.E. Sanders and R.M. Kiehn, IEEE J. Quant. Electron. QE-13 (1977) 739.
[2] R.C. Jones, J. Opt. Soc. Am. 31 (1941) 488; 32 (1942) 486.

*U.S.Government Printing Office: 1980 — 657-084/500